

UNCLASSIFIED

AD **405 125**

DEFENSE DOCUMENTATION CENTER

FOR

SCIENTIFIC AND TECHNICAL INFORMATION

CAMERON STATION, ALEXANDRIA, VIRGINIA



UNCLASSIFIED

NOTICE: When government or other drawings, specifications or other data are used for any purpose other than in connection with a definitely related government procurement operation, the U. S. Government thereby incurs no responsibility, nor any obligation whatsoever; and the fact that the Government may have formulated, furnished, or in any way supplied the said drawings, specifications, or other data is not to be regarded by implication or otherwise as in any manner licensing the holder or any other person or corporation, or conveying any rights or permission to manufacture, use or sell any patented invention that may in any way be related thereto.

405125

AFSWC-TDR-63-15

SWC
TDR
63-15

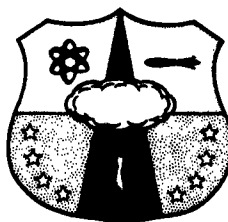
63-3-5

ZIRCONIUM — URANIUM COMBUSTION STUDY

(December 4, 1961 — December 3, 1962)

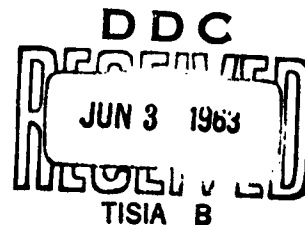
Final Report
April 1963

TECHNICAL DOCUMENTARY REPORT NUMBER AFSWC-TDR-63-15



Development Directorate
AIR FORCE SPECIAL WEAPONS CENTER
Air Force Systems Command
Kirtland Air Force Base
New Mexico

Project No. 1831, Task No. 183101



(Prepared under Contract AF 29(601)-4954
by Fred E. Littman, Stanford Research
Institute, Menlo Park, California)

405125

**HEADQUARTERS
AIR FORCE SPECIAL WEAPONS CENTER
Air Force Systems Command
Kirtland Air Force Base
New Mexico**

When Government drawings, specifications, or other data are used for any purpose other than in connection with a definitely related Government procurement operation, the United States Government thereby incurs no responsibility nor any obligation whatsoever; and the fact that the Government may have formulated, furnished, or in any way supplied the said drawings, specifications, or other data, is not to be regarded by implication or otherwise as in any manner licensing the holder or any other person or corporation, or conveying any rights or permission to manufacture, use, or sell any patented invention that may in any way be related thereto.

This report is made available for study upon the understanding that the Government's proprietary interests in and relating thereto shall not be impaired. In case of apparent conflict between the Government's proprietary interests and those of others, notify the Staff Judge Advocate, Air Force Systems Command, Andrews AF Base, Washington 25, DC.

This report is published for the exchange and stimulation of ideas; it does not necessarily express the intent or policy of any higher headquarters.

Qualified requesters may obtain copies of this report from ASTIA. Orders will be expedited if placed through the librarian or other staff member designated to request and receive documents from ASTIA.

FOREWORD

Many people have contributed to this study, and this report is but the sum total of these efforts. In particular, Mr. Arthur Reed, who operated the arc image furnace, and Mr. Dante Petro, who spent many hours developing satisfactory metallographic techniques, are largely responsible for the success of this study. The importance of the Technical Meetings of the contractors of Project 1831, who, under the auspices of the AFSWC Project Officers, guided the over-all direction of these studies, can hardly be overestimated and is gratefully acknowledged.

This report is further identified by the contractor's project number, PMU-3920

ABSTRACT

This investigation was designed to provide an experimental verification of the melting and oxidation behavior of fuel rod material of the type used in SNAP-2 and SNAP-10A auxiliary power reactors. Samples of zirconium-uranium alloy, both hydrided and unhydrided, were subjected to static conditions approximating re-entry trajectories. Heat flux and pressure conditions encountered during re-entry were selected to bracket ballistic parameter ranges of $W/C_D A = 20$ to $W/C_D A = 300$ and altitude ranges of 400,000 to 150,000 feet. An arc image furnace capable of delivering up to 900 BTU/ft²-sec was used as a source of radiant flux.

The results suggest that under these conditions no melting of the fuel rods is likely to occur. The material lost hydrogen and became almost completely oxidized. The resulting material, though mechanically weaker and more brittle than the starting material, was also extremely refractory owing to the high melting point of the zirconium oxide.

PUBLICATION REVIEW

This report has been reviewed and is approved.



M. E. SORTE
Colonel USAF
Director, Development Directorate



JOHN J. DISHUCK
Colonel USAF
DCS/Plans & Operations

CONTENTS

I	INTRODUCTION	1
II	SUMMARY	2
III	EXPERIMENTAL	3
	A. Equipment and Procedure	7
	1. Arc Image Furnace	7
	2. Experimental Procedure	8
	3. Metallography	9
	B. Experimental Results	9
	1. Preliminary Runs	9
	2. Simulation of "a" Trajectories	10
	3. Simulation of "b" Trajectories	14
	4. Formation of Water	16
	5. Emissivity Measurements	17
IV	CONCLUSIONS AND RECOMMENDATIONS	19
	DISTRIBUTION	52

LIST OF ILLUSTRATIONS

Fig. 1	"a" Trajectories ($W/C_D A = 20 \text{ lb/ft}^2$)	20
Fig. 2	"b" Trajectories ($W/C_D A = 300 \text{ lb/ft}^2$)	21
Fig. 3	Schematic Diagram of Arc Image Furnace	22
Fig. 4	Arc Image Furnace and Auxiliary Equipment	23
Fig. 5	Adjustable Diaphragm	24
Fig. 6	High Pressure Container	25
Fig. 7	Typical Sample	26
Fig. 8	Calibration Curve for Arc Image Furnace	27
Fig. 9	Zirconium - 10% Uranium Alloy	28
Fig. 10	Hydrided Zirconium - Uranium Alloy	29
Fig. 11	Photomicrographs of Heated and Oxidized Zirconium	30
Fig. 12	a and b Zirconium - Uranium Alloy after Heating	31
Fig. 13	a and b Zirconium - Uranium Hydride after Heating	31
Fig. 14	"a" Trajectory (400,000 ft)	32
Fig. 15	Samples of Material from "a" Trajectory	33
Fig. 16	"1a" Trajectory (300,000 ft)	34
Fig. 17	Samples of Material from "1a" Trajectory	35
Fig. 18	"2a" Trajectory (250,000 ft)	36
Fig. 19	Samples of Material from "2a" Trajectory	37
Fig. 20	"3a" Trajectory (200,000 ft)	38
Fig. 21	Samples of Material from "3a" Trajectory at Average Stagnation Flux	39

LIST OF ILLUSTRATIONS (Concluded)

Fig. 22	Samples of Material from "3a" Trajectory at Increased Flux	40
Fig. 23	"4a" Trajectory (150,000 ft)	41
Fig. 24	Samples of Material from "4a" Trajectory	42
Fig. 25	"b" Trajectory (400,000 ft)	43
Fig. 26	Samples of Material from "b" Trajectory	44
Fig. 27	"1b" Trajectory (300,000 ft)	45
Fig. 28	Samples of Material from "1b" Trajectory	46
Fig. 29	"2b" Trajectory (250,000 ft)	47
Fig. 30	Samples of Material from "2b" Trajectory	48
Fig. 31	"3b" Trajectory (200,000 ft)	49
Fig. 32	Samples of Material from "3b" Trajectory	50
Fig. 33	Formation of Water	51

LIST OF TABLES

Table I	Flux and Pressure Conditions for Selected Trajectories: Normal Trajectories	5
Table II	Flux and Pressure Conditions for Selected Trajectories: Axial Trajectories	6
Table III	Total Stagnation Point Heating of Exposed Fuel Elements	7
Table IV	Simulation of "a" Trajectory	11
Table V	Simulation of "1a" Trajectory	12
Table VI	Simulation of "2a" Trajectory	12
Table VII	Simulation of "3a" Trajectory	13
Table VIII	Simulation of "4a" Trajectory	14
Table IX	Simulation of "b" Trajectory	15
Table X	Simulation of "1b" Trajectory	16
Table XI	Simulation of "2b" Trajectory	16
Table XII	Simulation of "3b" Trajectory	17

I INTRODUCTION

When nuclear-powered energy sources are carried in aerospace vehicles, it will be necessary to dispose of them or recover them at the end of their projected flights. Incineration during their re-entry into earth's atmosphere has been considered as a practical means of safe disposal, provided that this process results in particles small enough to remain suspended for a long time or to become sufficiently dispersed.

The present Air Force task (183101) under Project No. 1831, was devised specifically to obtain information regarding the burn-up of nuclear auxiliary power systems of the SNAP 10A and 2 type, which are compact nuclear reactors in which zirconium-uranium hydride fuel elements are used. These fuel elements (and the fission product inventory they contain at the end of the projected life) constitute the main hazard of radioactive contamination, if they should reach the earth intact.

This study was an experimental investigation of the fate of a zirconium-uranium hydride fuel elements subjected to simulated re-entry conditions of stagnation heating and pressures. Its purpose was to determine, insofar as possible with available laboratory apparatus and reasonable effort, the melting and oxidation behavior of this material, to obtain information on the particle size of the resulting products of combustion, and to establish a generalized model of the behavior of fuel rod material under re-entry conditions.

II SUMMARY

Samples of hydrided and unhydrided fuel rod material (90% Zr-10% U) were exposed to heat fluxes and pressures simulating a variety of re-entry trajectories characteristic of a satellite returning in a decaying orbit. The temperature which the sample reached under these conditions was measured and the reacted samples were examined microscopically. The results obtained suggest that hydrided zirconium-uranium fuel elements will not melt or disintegrate under these conditions. Although temperatures up to the melting point of zirconium ($\sim 3850^{\circ}\text{R}$) were reached, incipient melting occurred under only one set of conditions. There was no evidence of formation of a liquid layer. This was probably due to the simultaneous formation of an oxide (and nitride) layer on the surface; such a layer would be highly refractory (the melting point of zirconium dioxide is $\sim 5340^{\circ}\text{R}$).

The rapid loss of hydrogen on heating resulted in a weakening of the mechanical strength of the material, both directly through the formation of numerous cracks and fissures, and indirectly by internal oxidation, leading to the friable oxide. Oxidation was enhanced only in runs that simulated trajectories of considerable duration, when the samples remained hot and in contact with air after the evolution of hydrogen had ceased. In the case of short-term trajectories, resulting from low-altitude ejection, the evolving hydrogen effectively protected the sample from oxidation, though cracking did, of course, occur. The cracking appeared to be due to the 10% reduction in volume accompanying dehydrogenation.

The evolving hydrogen combined with oxygen to form steam, at least at higher ambient pressure. This reaction apparently took place on the surface of the sample.

III EXPERIMENTAL

At the Technical Working Group Meeting held at General Dynamics/Astronautics in San Diego on April 3-6, 1962, the re-entry conditions were agreed on. In order to bracket reentry conditions likely to be met in practice, it was decided to investigate conditions encountered by an object re-entering in a polar orbit starting at the north pole, having a velocity of 25,680 ft/sec, a zero entering angle, and a ballistic parameter $W/C_D A$ of 20 (rod normal to trajectory) and 300 (rod axial) lb/sq ft. It was further assumed that for each ballistic parameter the ejection of the fuel rods would occur at each of these altitudes: 400, 300, 250, 200, 150, or 100 K ft; for convenience the trajectories were designated the "a" and "b" series according to the following scheme.

Ejection Ht (K ft)	Trajectory	
	$W/C_D A=20$	$W/C_D A=300$
400	a	b
300	1a	1b
250	2a	2b
200	3a	3b
150	4a	4b
100	5a	5b

In the heat transfer calculations, a cold wall temperature of 500°R was assumed. This assumption tends to make the calculated flux higher than that to be expected in practice. These trajectories and the corresponding instantaneous and accumulated flux were to be calculated by GD-Astronautics and distributed to the interested contractors.

The trajectories and heat transfer calculations became available in June and were used to determine a series of flux and pressure conditions simulating those undergone by a fuel rod ejected at several altitudes during re-entry. Samples of zirconium-uranium alloy, both hydrided and unhydrided, were then subjected to treatments simulating these conditions. The flux and pressure conditions of the two families of trajectories are shown in Fig. 1 and 2. The flux data were obtained directly from Figs. 4-6 of General Dynamics Quarterly Report No. 3. The stagnation pressures corresponding to these conditions were calculated from ambient pressures and corresponding to these conditions were calculated from ambient pressures and the corresponding Mach number according to¹

¹ M. G. Meyer, Real Gas Equilibrium Properties, Lockheed No. LMSO-TXA-111 (1961)

$$P_{st} = 1.348 M_{\infty}^2 P_{\infty}$$

where P_{st} designates the stagnation pressure, M_{∞} the ambient Mach number, P_{∞} the ambient pressure. The data, based on the ARDC Model Atmosphere (1959) are shown in Tables I and II. The "5a," "4b," and "5b" trajectories were not included in the experimental approach, because in those trajectories the total integrated heat content drops to a very low figure, as was pointed out by Philbin² in the listing shown in Table III. The amount of heat required to melt a 1.25-inch fuel element is of the order of 2,400 Btu.³

For experimental simulation of the trajectories, both the flux and the pressure values were averaged over periods of time ranging from 300 to 20 seconds, depending on the slope of the curves, as shown in the accompanying diagrams (e.g., Fig. 14). Thus the continuous curve of flux and stagnation pressure was approximated by a step function. The actual flux used was increased by 50% in most runs to compensate for two factors: the experimental conditions, which permitted the heating of one face of the sample only while at the same time it was radiating from five sides; and, offsetting this to some extent, the reduction of stagnation point flux to average flux by a factor of three due to the tumbling of the rod. Because of the small sample size, the relatively long heating periods, and the experimental arrangement, it can be assumed that the sample is at substantially uniform temperature and that all heat loss is by radiation. Under these circumstances the required arc flux is obtained by simply equating the cold wall input of the arc (thus compensating to some extent for the cold wall assumption noted above in the heat transfer calculations) to the stagnation heating of a rod rotating at more than about 1 cps.⁴

$$\epsilon \dot{q}_i A_i = \frac{1}{3} q_s A_t$$

where ϵ is the emissivity, q heat flux, A area, and the subscripts i , s , and t refer to arc image input, stagnation, and total. With $\epsilon = 0.8$ ⁵ and our particular wedge-shaped sample ($A_i/A_t = 0.275$), we find $q_i = 1.5 q_s$, requiring a 50% increase in incident flux.

² Philbin, E. J. Re-entry and Disposal Phenomena for NAPS - Third Quarterly Report. (AE62-0683) General Dynamics/Astronautics

³ Zlotnick, M., et al. Investigation of Re-entry Destruction of NAPS (AFSWC-TR-61-69), AVCO Corp., Wilmington, Mass. (RAD-TR-61-28)

⁴ Philbin, E. J. Re-entry and Disposal Phenomena for NAPS - Fifth Quarterly Report. (AE 63-0011) General Dynamics/Astronautics.

⁵ Furman, S. C. and P. A. McManus. Metal Water Reactions. IX. (GEAP-3338) Vallecitos Atomic Lab., General Electric Co.

Table I
FLUX AND PRESSURE CONDITIONS FOR SELECTED TRAJECTORIES
NORMAL TRAJECTORIES($w/c_D=20$)

Altitude (kilofeet) Nominal Actual [†]		Time From Re-Entry (sec)	Time From Ejection (sec)	Mach No.	Pressure,* Ambient (inches Hg)		Pressure,* Stagnation (inches Hg)		Flux, Stagna- tion (Btu/ ft ² -sec)
"a" Trajectory									
400	400	0	0	17.0	5.3	-7	2.0	-4	5
<u>350</u>	347	800	800	26.0	2.6	-6	2.6	-3	20
300	297	1150	1150	29.9	3.6	-5	4.4	-2	75
250	248	1325	1325	26.2	6.9	-4	6.4	-1	270
200	197	1400	1400	16.3	7.5	-3	2.7	0	240
150	140	1450	1450	6.5	6.3	-2	3.6	0	20
100	92	1500	1500	1.2	4.7	-1	-	-	0
50	51	1575	1575	0.3	3.3	0	-	-	-
"1a" Trajectory									
300	298	1300	0	30.2	3.6	-5	4.5	-2	100
<u>250</u>	250	1575	275	26.3	6.2	-4	5.7	-1	310
200	200	1650	350	16.8	6.7	-3	2.5	0	350
150	150	1695	395	7.9	4.3	-2	3.6	0	80
100	98	1745	445	1.6	3.6	-1	-	-	0
50	50	1830	530	0.4	3.3	0	-	-	-
"2a" Trajectory									
<u>250</u>	252	1825	0	28.6	8.5	-4	6.1	-1	380
<u>200</u>	199	1950	125	16.2	6.9	-3	2.5	0	325
150	150	1995	170	7.8	4.3	-2	3.6	0	95
100	102	2040	215	1.9	3.0	-1	-	-	0
50	50	2130	305	0.4	3.3	0	-	-	-
"3a" Trajectory									
<u>200</u>	204	2000	0	23.5	5.6	-3	4.2	0	900
<u>150</u>	151	2075	75	7.6	4.2	-2	3.3	0	80
100	101	2125	125	1.8	3.1	-1	-	-	0
50	50	2210	210	0.4	3.3	0	-	-	-
"4a" Trajectory									
<u>150</u>	158	2075	0	19.6	3.2	-2	1.7	1	760
<u>100</u>	101	2150	75	1.6	3.1	-1	-	-	0
50	51	2235	160	0.4	3.3	0	-	-	-

*Number following initial entry indicates power of ten multiplicand

†Nearest datum point furnished by computer

Table II
FLUX AND PRESSURE CONDITIONS FOR SELECTED TRAJECTORIES
AXIAL TRAJECTORIES ($W/C_A = 300$)

Altitude (kilofeet) Nominal Actual†		Time From Re-Entry (sec)	Time From Ejection (sec)	Mach No.	Pressure,* Ambient (inches Hg)			Pressure,* Stagnation (inches Hg)		Flux, Stagna- tion (Btu/ ft²-sec)
"b" Trajectory										
400	400	0	0	17.0	5.3	-7	2.1	-4	5	
350	350	300	300	25.8	2.2	-6	2.0	-3	10	
300	298	1300	1300	30.2	3.8	-5	4.7	-2	50	
250	252	2000	2000	23.5	5.6	-3	4.2	0	470	
150	158	2075	2075	19.6	2.2	-2	1.1	1	730	
100	109	2125	2125	14.6	2.2	-1	6.3	1	480	
50	57	2175	2175	3.2	2.5	0	3.5	1	10	
"1b" Trajectory										
300	297	1150	0	29.9	3.6	-5	4.3	-5	50	
250	250	1350	200	28.4	6.2	-4	6.7	-1	200	
200	201	1480	330	23.4	6.4	-3	4.7	0	490	
150	149	1580	410	19.2	4.5	-2	2.2	1	780	
100	98	1610	460	12.1	3.6	-1	7.1	1	400	
50	49	1660	510	2.2	3.6	0	2.3	1	10	
"2b" Trajectory										
250	249	1325	0	26.3	6.9	-4	6.5	-1	160	
200	199	1400	75	22.0	6.9	-3	4.5	0	430	
150	149	1450	125	19.1	4.5	-2	2.2	1	800	
100	100	1490	165	13.3	3.3	-1	7.8	1	450	
50	49	1540	215	2.2	3.6	0	2.3	1	10	
"3b" Trajectory										
200	197	1400	0	16.3	7.5	-3	2.7	0	180	
150	152	1435	35	14.9	40	-2	1.2	1	320	
100	102	1465	65	12.6	3.0	-1	6.4	1	440	
50	51	1505	105	2.7	3.3	0	3.2	1	5	

*Number following initial entry indicates power of ten multiplicand

†Nearest datum point furnished by computer

Table III
TOTAL STAGNATION POINT HEATING OF EXPOSED
FUEL ELEMENTS

Trajectory	Total Heating (Btu/ft ²)	Trajectory	Total Heating (Btu/ft ²)
a	60 x 10 ³	b	202 x 10 ³
1a	61 x 10 ³	1b	153 x 10 ³
2a	42 x 10 ³	2b	89 x 10 ³
3a	22 x 10 ³	3b	29 x 10 ³
4a	9 x 10 ³	4b	3 x 10 ³
5a	2 x 10 ³	5b	0.1 x 10 ³

A. Equipment and Procedure

1. Arc Image Furnace

The major piece of equipment used is an arc image furnace equipped with 14-inch elliptical mirrors. This apparatus, a lineal descendant of the mirror system used by Archimedes in 212 B.C. to burn the ships of the invading Roman navy at Syracuse, consists of a carbon arc system as a source of energy, and a pair of elliptical mirrors whose function is to collect and transfer this energy to another plane, the "furnace" area. Flux densities of the order of 900 Btu/ft²-sec can easily be obtained by commercial equipment and maintained for 20-30 minutes, the lifetime of a carbon electrode. These flux densities correspond to a black body temperature of over 5000°R. Control of the flux density can best be achieved by decreasing the area of the subtended angle of the secondary mirror by means of continuous or step diaphragms.

The sample rested on a zirconia column, which was contained in a borosilicate glass exposure chamber. For experiments at less than atmospheric pressure, a thin-walled, spherical container was used, which did not absorb a measurable amount of radiant energy. For high pressure experiments, a thick-walled glass container was used, which reduced the incident energy by about 20%. Fig. 3 shows a schematic diagram of the equipment, Fig. 4 an over-all view, Fig. 5 a detail of the adjustable diaphragm and sample container. Fig. 6 shows the high pressure container, Fig. 7 a close-up of a typical sample.

The furnace was calibrated with a radiometer developed by the Naval Defense Radiological Laboratories. This meter consists essentially of a small blackened silver disk, to which a thermocouple is connected. The disk is embedded in a water-cooled copper block, which constitutes an infinite heat sink. The temperature reached by the black target is directly proportional to the heat input; the instrument is calibrated

TDR-63-15

in terms of millivolt output per Btu/ft²-sec flux having a constant of 41.6 Btu/ft²-sec-mv. Fig. 8 shows the results obtained by using this meter for two different sets of mirrors. The new mirrors were used for all experiments requiring high flux levels.

Pressures were measured with an assortment of gages, depending on the desired range. A McLeod gage was used for pressures up to 0.1 inch, a manometer up to atmospheric pressure, and a Bourdon gage for higher pressures. Pressure, as well as flux, was changed stepwise as indicated on the diagrams representing the several trajectories.

Optical measurement of temperatures proved to be quite difficult because reflection of the arc on the surface of the sample resulted in high readings. The problem was eventually solved by using a Micro Pyrometer, which was focused on a hole 0.025-inch in diameter and 0.150-inch deep, drilled into the side of the sample. The hole can be seen clearly in Fig. 7. Drilling holes into the hydrided samples was exceedingly difficult, but was eventually accomplished with a supersonic drill. The temperature readings thus obtained closely approximate black body temperatures, since it can be shown that an apparent emissivity of 0.99 results with a hole having a depth of 2.6 diameters and a surface emissivity of 0.75.⁶

2. Experimental Procedures

Except for a few early runs in which cubic samples were used, the samples were wedge-shaped, approximately 3/16 inch on edge. Two types of material were used: zirconium-10% uranium alloy, and hydrided material of the same starting composition, containing about 1.9 atoms of hydrogen per atom of zirconium. The uranium was not enriched, so no special precautions were required in handling it. Typical photomicrographs of the starting material are shown in Fig. 9 and 10. The alloy has a very fine crystal structure, without characteristic markings. The hydrided material shows very large, banded crystals, characteristic of hydrides containing more than 1.6 atoms of hydrogen per atom of zirconium.

The alloy was easily cut and drilled by conventional cutting tools. The hydride, being hard and brittle, was cut with a wet carborundum wheel, and drilled by a supersonic drill, as mentioned previously. The filings of hydrided material were pyrophoric; the alloy did not appear to be.

Once the furnace was calibrated, the sample, resting on a zirconia column, was positioned in the exact focus by means of a jig. The pressure was then adjusted to correspond to the first step of the trajectory which was to be simulated. The proper flux was assured by a corresponding setting of the diaphragm. The arc was then lit and exposure was begun by using a shutter. Changes from one level to the

⁶ Sparrow, E. M. et al., Radiation Characteristics of Cylindrical Enclosures, J. Heat Transfer 1962, pp 73-81.

TDR-63-15

next were made as rapidly as possible by adjusting a bleeder valve and the diaphragm, without dowsing the arc.

Temperature readings were taken at frequent intervals and an average reading was recorded for each step. The sample was closely observed through the telescope of the Micro Pyrometer during the run.

When it became apparent that moisture formed and condensed on the walls of the containing vessel under certain conditions, motion pictures of this action were taken at a 64-frames/sec frequency. Kodachrome film was used for this record.

3. Metallography

Surface preparation of zirconium alloy samples is quite tricky, because it tends to "smear." A number of grinding and polishing techniques were tried. The following seemed to give the best results.

The samples were mounted in cold-set plastic, about 1/16-inch was ground off to remove strained material, and the resulting face was polished on 600-grit silicon carbide paper. The polish marks were removed with a chemical etch consisting of 47% nitric acid (65%), 5% hydrofluoric acid (48%), and 48% hydrogen peroxide (3%). The etching solution was applied with a cotton swab, and rinsed off after 10-15 seconds with distilled water. If necessary, the etching was repeated until a satisfactory surface was obtained. The sample was then rinsed in methanol and dried with warm air. It had to be examined within 1-2 hours, since an oxide coating seemed to form overnight. Typical metallographs of the structure of the alloy and hydride as received are shown in Figs. 9 and 10.

In general, it appeared that the less the samples were "worked" the better the results. The surfaces obtained by the method described were reproducible.

X-ray diffraction analyses were run on a number of early samples, but did not seem to provide much information, primarily because the equipment used "sees" all of the sample at once and therefore produces an integrated result.

B. Experimental Results

1. Preliminary Runs

The uranium-zirconium alloy and hydride samples did not become available until April. Some preliminary work was therefore performed with reactor grade zirconium, of which a supply was on hand.

In the first series of experiments, a zirconium target 0.030-inch thick and 3/8-inch in diameter was used. The sample was placed in the focus of the arc-image furnace at an incident flux level of the order

TDR-63-15

of 250-300 Btu/ft²-sec for about 30 seconds. The first sample was heated in air at atmospheric pressure. It became covered with a white oxide, but did not melt. Metallographic examination showed that the sample was completely converted to zirconium oxide (Fig. 11a).

Another sample was enclosed in a Vycor tube and maintained at 100 mm pressure of air. It was heated similarly. It did not melt, but became covered with a dark oxide layer. Metallographic examination showed an oxide case to the depth of about 10% of the sample and conversion of the remaining metal to β -zirconium. Extensive internal cavitation was present (Fig. 11b).

The third sample was heated in an evacuated, sealed Vycor tube. This sample partially melted; the remaining zirconium retained the structure of α -zirconium (Fig. 11c).

From the foregoing it appears that partial or complete oxidation of zirconium inhibits the melting of zirconium samples (the oxide melts 1650°F higher than the metal). Oxidation also stabilizes the β -phase of zirconium. The oxidation is slow enough, moreover, that it does not become self-sustaining (at atmospheric pressure), even when the sample is heated by an incident flux of the order of 250 Btu/ft²-sec.

In another series with zirconium the targets were cubes measuring about 3/16-inch on each side. The cubes were supported on an alumina rod in air and heated at different fluxes to equilibrium temperatures. As heating progressed, the samples oxidized heavily, becoming covered with a white, nonadhering oxide layer which rapidly thickened, until the whole sample was transformed into oxide.

The first tests of zirconium-uranium alloy were also performed with cubes (3/16-inch). On heating in air at atmospheric pressure, the samples showed a behavior similar to that of the zirconium samples. The unhydrided material oxidized quietly, without melting, at fluxes from 100 to 600 Btu/ft²-sec. The hydrided samples behaved similarly at low flux densities, oxidizing quietly and developing numerous fissures. At high flux densities, sudden eruptions occurred, resulting in the spilling of molten metal from the inside of the cube. The metal quickly solidified and became converted into an oxide. Marked cavitation inside the cubes was noted.

The appearance of the reacted samples at a flux of about 600 Btu/ft²-sec, both from the outside and after sectioning, is shown in Figs. 12 and 13.

2. Simulation of "a" trajectories

The first set of trajectories to be simulated were the "a" trajectories, corresponding to the flight path of an object having a ballistic parameter $W/C_D A$ of 20 lb/ft². They are characteristic of the conditions encountered by a fuel rod ejected from the reactor at various altitudes in a normal orientation, that is, with their long axis perpendicular to the direction of flight.

TDR-63-15

A graph of the "a" trajectory (ejection altitude 400,000 ft) and the appearance of typical samples subjected to the conditions detailed in Table IV are shown in Figs. 14 and 15. The samples show a much larger grain structure than the starting material and a characteristic columnar structure on the oxidized surface. The hydrided sample shows no traces of the original structure and is honeycombed with voids. There is no evidence of oxidation.

In Table IV and all of the tables to follow, \dot{q}_s denotes the average stagnation flux calculated for the time interval in question (in the

Table IV

SIMULATION OF "a" TRAJECTORY

Time (sec)	Pressure (inches Hg)	Flux (Btu/ft ² -sec)		Temperature (°R)			
		\dot{q}_s	\dot{q}_1	Alloy a-6	Alloy a-7	Hydride a-8	Hydride a-9
300		45	68	2255	2330	2255	2200
100	0.04	90	145	2530	2690	2330	2240
100	0.24	200	300	3100	3190	2580	2510
100	1.40	340	510	3390	3500	3030	3010
100	2.40	140	210	2740	2800	2310	2320

present case shown in Fig. 14) and \dot{q}_1 the actual (with some exceptions to be noted below) input flux, increased to compensate for the difference between aerodynamic heating and radiative heating of only one surface, as discussed above.

The "1a" trajectory (ejection at 300,000 ft) was run similarly. The trajectory and the appearance of the reacted samples are shown in Figs. 16 and 17. The samples are quite similar to the previous ones in appearance: again there are large crystals with a martensitic fine structure, columnar crystals around the edges of the sample, and the characteristic voids in the hydride sample. The large round cavity in the alloy sample is a drilled hole. There seems to be a thin oxide coating around the periphery of both samples. Data on simulation of the "1a" trajectory are shown in Table V.

The "2a" trajectory (ejection at 250,000 ft), Fig. 18, was also run at higher flux. Again there was the same characteristic behavior of the samples: there was no melting, the temperature attained by the hydrided sample was about 200°R lower than for the alloy, and there was a fairly rapid dehydrogenation evidenced at times by a movement of the sample on

Table V
SIMULATION OF "1a" TRAJECTORY

Time (sec)	Pressure (inches Hg)	Flux (Btu/ft ² -sec)		Temperature (°R)					
		\dot{q}_s	\dot{q}_1	Alloy 1a-5	Alloy 1a-6	Alloy 1a-7	Hydride 1a-8	Hydride 1a-9	Hydride 1a-10
100	0.1	110	165	2615	2850	2940	2420	2260	2260
100	0.2	150	225	2760	2870	3050	2580	2350	2370
100	0.6	265	395	3050	3230	3260	3190	2740	2795
50	2.0	365	545	3335	3445	3515	3500	2940	3050
50	4.0	215	120	2850	3155	3190	3140	2600	2635
50	2.6	45	25	2220	2200	2200	2260	2220	2240

its pedestal. The photomicrographs (Fig. 19) showed very little change in the appearance of the alloy, only dehydrogenation of the hydrided sample. Data for the simulated trajectory are in Table VI.

Beginning with the "3a" trajectory, the shape of the heat pulse changes. Instead of a maximum-type curve, we now have a decaying pulse,

Table VI
SIMULATION OF "2a" TRAJECTORY

Time (sec)	Pressure (inches Hg)	Flux (Btu/ft ² -sec)		Temperature (°R)			
		\dot{q}_s	\dot{q}_1	Alloy 2a-5	Alloy 2a-6	Alloy 2a-7	Hydride 2a-8
50	0.8	365	545	-	3100	2970	2830
50	1.0	360	540	-	2995	3010	2850
50	1.9	265	395	2740	2650	2670	2615
50	3.7	100	150	2260	2260	2240	2260
50	1.6	10	15	2040	2095	2095	2132

TDR-63-15

starting off at high values and dropping off rapidly. The total integrated heat content, represented by the area under the curve, decreases very rapidly as ejection occurs at successively lower altitudes. The trajectory and photomicrographs of the samples are shown in Fig. 20, 21, and 22. Figure 21 shows the appearance of a run made at \dot{q}_s . The hydride sample (No. 3a-3) is of particular interest, as it shows a transition of hydrided to unhydrided material. The "regular" sample of hydride, run at the higher flux level \dot{q}_i reached a temperature almost 360°R higher. The alloy sample resembled (3a-2) run at lower flux levels, showing only a thin, adhering oxide layer and no profound changes in the metal. The hydrided sample showed a pattern of fine fissures, rather uniformly distributed through the sample (Fig. 22). Data are shown in Table VII.

Table VII
SIMULATION OF "3a" TRAJECTORY

Time (sec)	Pressure (inches Hg)	Flux (Btu/ft ² -sec)		Temperature ($^\circ\text{R}$)					
		\dot{q}_s	\dot{q}_i	Alloy 3a-2*	Alloy 3a-5	Alloy 3a-6	Hydride 3a-3*	Hydride 3a-7	Hydride 3a-8
20	4.5	700	900	3500	3480	3895	3140	3535	3515
20	4.0	340	510	3320	2960	3010	3010	2060	2995
20	4.4	160	240	2545	2260	2420	2400	2385	2400
20	3.9	40	60	2420	2110	2110	2310	2145	2185

*Run at \dot{q}_s

The "4a" trajectory has an even shorter history of exposure--only 60 seconds (Fig. 23). Starting out with a strong heat pulse at relatively high gas pressures--almost an atmosphere--results in a distinct oxide layer on the outside of the alloy sample, followed by a layer of columnar crystals (Fig. 24). The interior of the sample shows little change. The hydrided sample lost hydrogen very rapidly under these conditions and shows a regular pattern of large fissures. It is noteworthy that there is no oxide formed on this sample, suggesting that the evolving hydrogen consumes all of the oxygen available at the surface of the sample. The data for this run are shown in Table VIII.

Table VIII
SIMULATION OF "4a" TRAJECTORY

Time (sec)	Pressure (inches Hg)	Flux (Btu/ft ² -sec)		Temperature (°R)			
		\dot{q}_s	\dot{q}_1	Alloy 4a-5	Alloy 4a-6	Hydride 4a-7	Hydride 4a-8
20	20.8	480	720	3715	3680	3370	3500
20	4.4	140	210	2330	2260	2220	2185
20	2.4	48	72	2110	2165	2145	2110

During several of the hydride runs simulating "3a" and "4a" trajectories, transient accumulation of moisture was noticed on the walls of the confining vessel. The phenomenon is described in more detail in section B-4.

3. Simulation of "b" Trajectories

The heating and pressure histories of fuel elements entering the atmosphere in an axial alignment to the trajectory differ considerably from those of elements entering in a crossflow position. The much higher value of the ballistic parameter $W/C_D A$ resulted not only in a higher heat flux but also in much higher stagnation pressures experienced by these elements. This in turn was conducive to more rapid oxidation of the samples; and since the resulting zirconium dioxide is a very refractory material, its presence counteracted the effects of the higher heat flux and prevented melting of the specimens.

Since above-atmospheric pressures were encountered in simulation of the "b" trajectory (Fig. 25), the high pressure reaction chamber (described earlier) was used. The alloy sample (Fig. 26) showed curiously little change other than a growth of grain size. A heavy oxide coating, which was apparently cohesive enough to prevent further damage, is in evidence. The hydrided material, on the other hand, was heavily oxidized, both externally and internally. This was undoubtedly due to the many fissures which developed on dehydriding, which made rapid oxidation possible. Data for this run are shown in Table IX.

The discrepancy in appearance of hydrided samples representing the "4a" and "b" trajectories, both of which were mechanically weakened by the extensive fissuring, appears to be due primarily to the duration of the run. The longer time available on the "b" trajectory permitted heavy oxidation of the dehydrided sample.

Table IX
SIMULATION OF "b" TRAJECTORY

Time (sec)	Pressure (inches Hg)	Flux (Btu/ft ² -sec)		Temperature (°R)			
		\dot{q}_s	\dot{q}_1	Alloy b-5	Alloy b-6	Hydride b-7	Hydride b-8
400	0.2	60	90	2470	2510	2530	2470
200	0.4	130	195	2650	2650	2635	2615
200	2.4	320	480	3085	3155	3335	3245
100	18.4	640	900	3640	3695	3820	3840
100	66.0	320	480	3085	3155	3065	3140

The "1b" trajectory (Fig. 27) was simulated with both calculated \dot{q}_s flux and 50% excess. An increase of temperature of about 200°R resulted from this change. The temperature reached at maximum flux was 3800°R--sufficient to cause melting of the front surface of the alloy sample, as can be seen in Fig. 28. The sample was also heavily oxidized. The hydrided sample, though badly broken up and oxidized, did not show any evidence of melting, having reached a maximum temperature of only 3680°R. The conditions are detailed in Table X.

The "2b" trajectory, shown in Fig. 29, is characterized both by a very high peak flux and pressure, and by a relatively short duration of the heat pulse (about 200 seconds). The photomicrograph of the alloy sample shows considerable oxidation, and that of the hydrided sample shows evidence of violent degassing, such as large cavities, but only a moderate amount of oxidation. The samples did not melt. Table XI gives details of conditions.

The "3b" trajectory (Fig. 31) is characterized by relatively high air pressures and moderately high flux levels, as well as a short overall duration. This combination of factors produced very little change in the alloy sample beyond a thin oxide layer and a layer of columnar crystals. Even the hydrided sample (Fig. 32) shows only moderate disruption, though it is pocked by small voids and fissures. There is remarkably little oxidation. Conditions for this run are shown in Table XII.

Table X
SIMULATION OF "1b" TRAJECTORY

Time (sec)	Pressure (inches Hg)	Flux (Btu/ft ² -sec)		Temperature (°R)					
		\dot{q}_s	\dot{q}_1	Alloy* 1b-1	Hydride* 1b-2	Alloy* 1b-3	Hydride* 1b-4	Alloy 1b-5	Hydride 1b-7
300	0.2	65	100	2370	2310	2310	2350	2110	2145
100	1.2	215	325	2470	2385	2490	2435	2760	2185
100	4.8	415	625	3085	2980	3120	3210	3660	3280
100	30.0	670	900	3640	3660	3640	3730	3800	3680
100	30.0	240	360	2510	2400	2565	2760	2740	2650

*Run at \dot{q}_s

4. Formation of Water

As mentioned in section B-3, condensation of steam on the walls of the containing vessel was observed in the simulation of trajectory "3a" and "4a." To explore this further, moving pictures were taken at 64 frames per second under conditions of rapid heating at near atmospheric pressure. The formation of steam, followed by subsequent condensation on the walls, is clearly shown in the film. In Fig. 33 a series of single frames from

Table XI
SIMULATION OF "2b" TRAJECTORY

Time (sec)	Pressure (inches Hg)	Flux (Btu/ft ² -sec)		Temperature (°R)		
		\dot{q}_s	\dot{q}_1	Alloy 2b-1	Alloy 2b-2	Hydride 2b-4
50	1.2	245	360	2565	2510	2290
50	8.8	450	675	3280	3320	2940
50	36.8	720	900	3515	3590	3550
50	62.0	400	600	3190	3210	3010

Table XII

SIMULATION OF "3b" TRAJECTORY

Time (sec)	Pressure (inches Hg)	Flux (Btu/ft ² -sec)		Temperature (°R)		
		\dot{q}_s	\dot{q}_1	Alloy 3b-1	Alloy 3b-2	Hydride 3b-4
35	10.4	250	375	2470	2580	2330
35	44.0	400	600	3300	3190	3010
35	50.4	240	360	2470	2435	2330

the film are shown. The first frame shows the sample on its pedestal at the start of irradiation (the rectangular object in the background is metal foil); in the second the glass enveloped is heavily covered with condensed steam. The following frames show gradual clearing as the envelope warmed. No flame was observed. It appears evident, however, that at least under the above-stated condition the hydrogen resulting from the decomposition of the hydride is oxidized, probably catalytically on the surface of the sample.

5. Emissivity Measurements

The emissivity of the re-entering fuel rod is of considerable interest because it has a large effect on the equilibrium temperature attained by the rod. When a radiative heat source (such as an image furnace) is used to simulate re-entry conditions, the emissivity, or more precisely its numerical equivalent, the absorptivity of the sample, also enters into the picture. As was pointed out earlier, an emissivity of 0.8 was assumed in arriving at a scaling factor of 150% for the incident flux. If both the "black body" and the "brightness" temperature of an object are known, its emissivity ϵ can be calculated⁵

$$\ln \epsilon = \frac{c_2}{\lambda} \left(\frac{1}{T} - \frac{1}{S} \right),$$

where

- ϵ = emissivity
- c_2 = 1.438 cm °K
- λ = wavelength in cm
- T = black body temperature, °K
- S = brightness temperature, °K

TDR-63-15

When an optical pyrometer is used, $\lambda = 6.5 \times 10^{-5}$ cm, since a narrow-band red filter is used in these instruments.

In our experiments the Micro Pyrometer was, as mentioned, normally focused on a small hole in the sample, which acted like a black body. It was hoped that by taking simultaneous surface temperature readings good values of emissivity could be obtained.

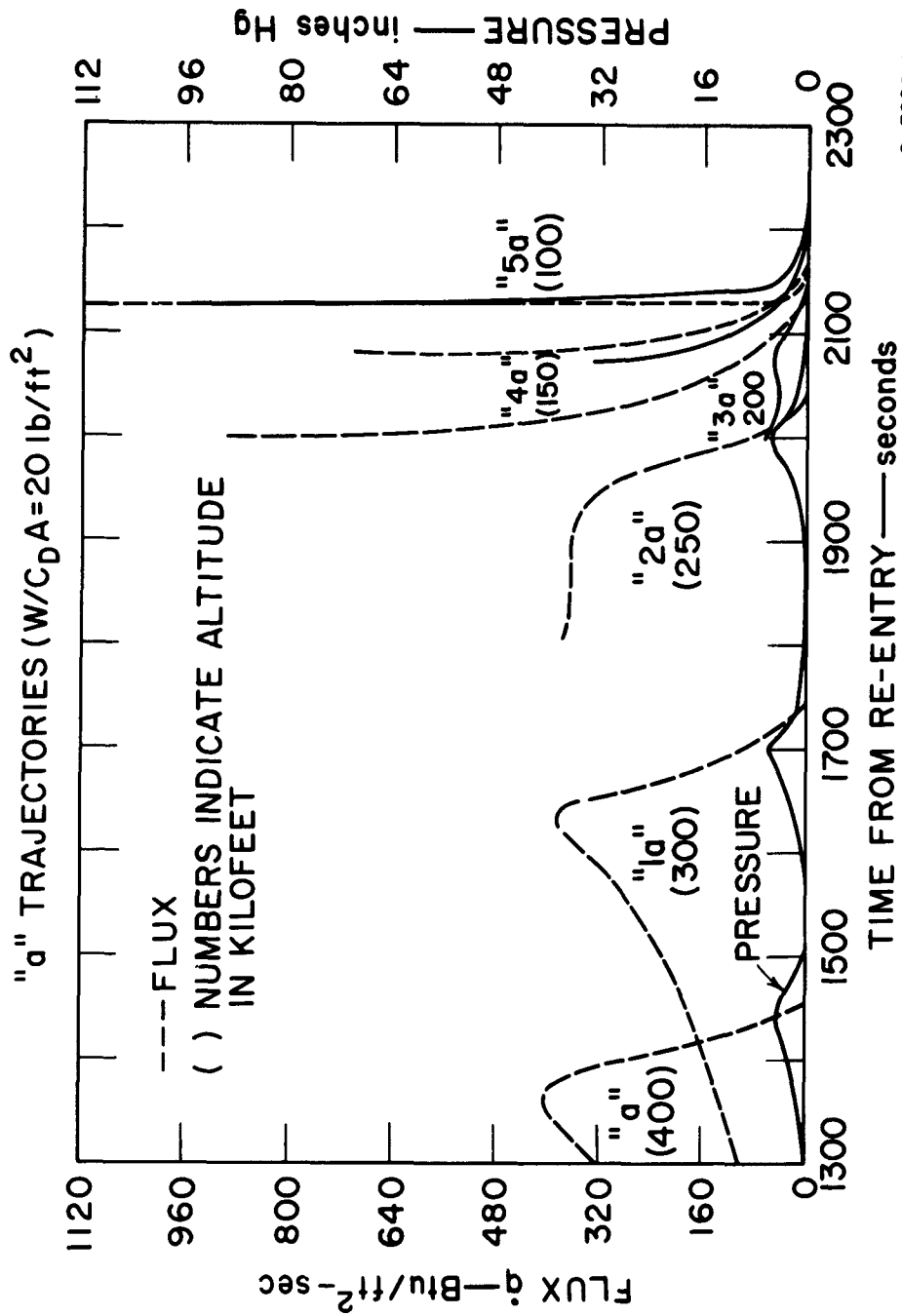
The procedure was in practice complicated by a number of factors, such as reflections from the reaction vessel, uneven temperature distribution, and the like. A considerable number of readings were taken under favorable circumstances and the emissivity was calculated. The average value obtained was about 0.65. However, this figure is given only for the record, it is not considered to be reliable, owing to the limitations mentioned above and in view of the General Electric results on zirconium oxide already cited and the recent results reported by Vidya⁷ for hydrided full rod material ($\epsilon \sim 0.78$ in the temperature range of interest).

⁷ Fleming, W. J. Liquid Layer Instability and Droplet Formation Study for Re-entering NAPS--Fourth Quarterly Progress Letter. Vidya Research and Development.

IV CONCLUSIONS & RECOMMENDATIONS

A considerable amount of evidence has been accumulated suggesting that hydrided zirconium-uranium alloy fuel elements will not melt and/or ablate when subjected to flux and pressure conditions simulating a variety of possible re-entry conditons. The conditions encountered seem to be right on the borderline; it is possible that in actual practice slightly higher fluxes would be produced and ablation would result. On the other hand, some of the assumptions made in the calculations of heating rates, such as cold-wall heat transfer, tend to give higher results than might be expected. In any case, it appears that there isn't a sufficient safety factor (asy, of the order of 2) to assure destruction of these elements by incineration.

It must be realized that the particular experimental approach taken deliberately neglected the effect of aerodynamic shear forces present under actual conditions. An evaluation of the possible effect of these forces, even from experiments under dynamic conditions such as a plasma jet stream, is very difficult because of the magnitude of the extrapolation required; from approximately sonic conditions to Mach 25 or 30.



C-3920-10RS

Figure 1

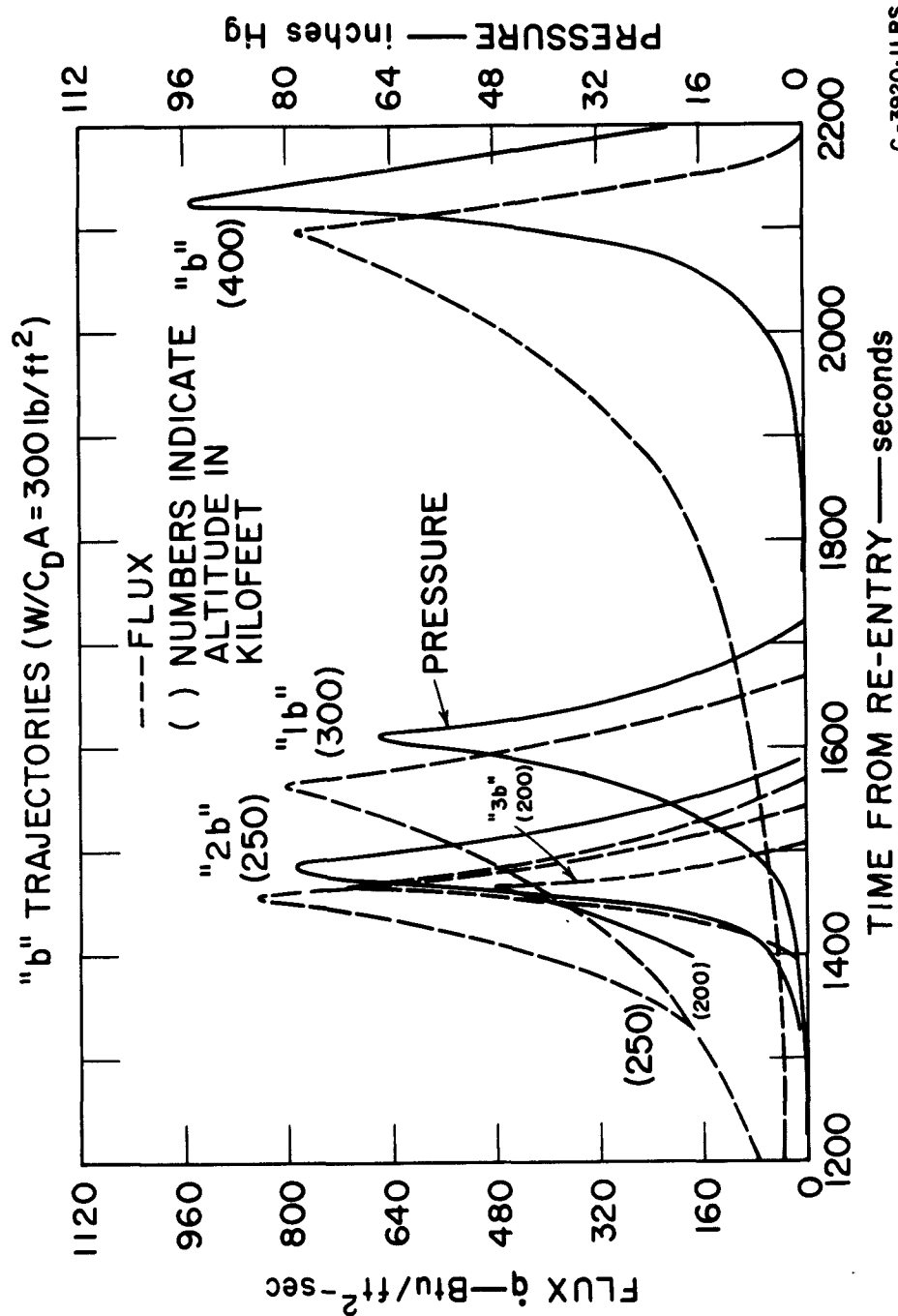
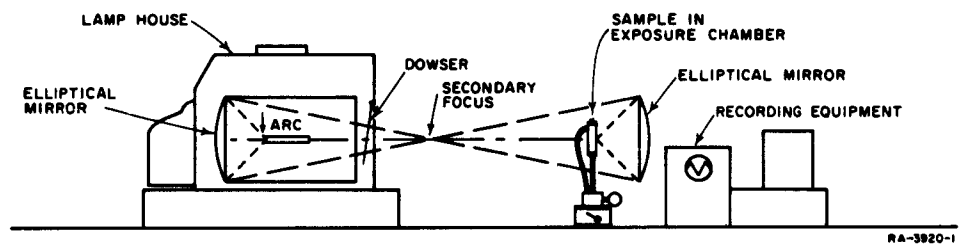
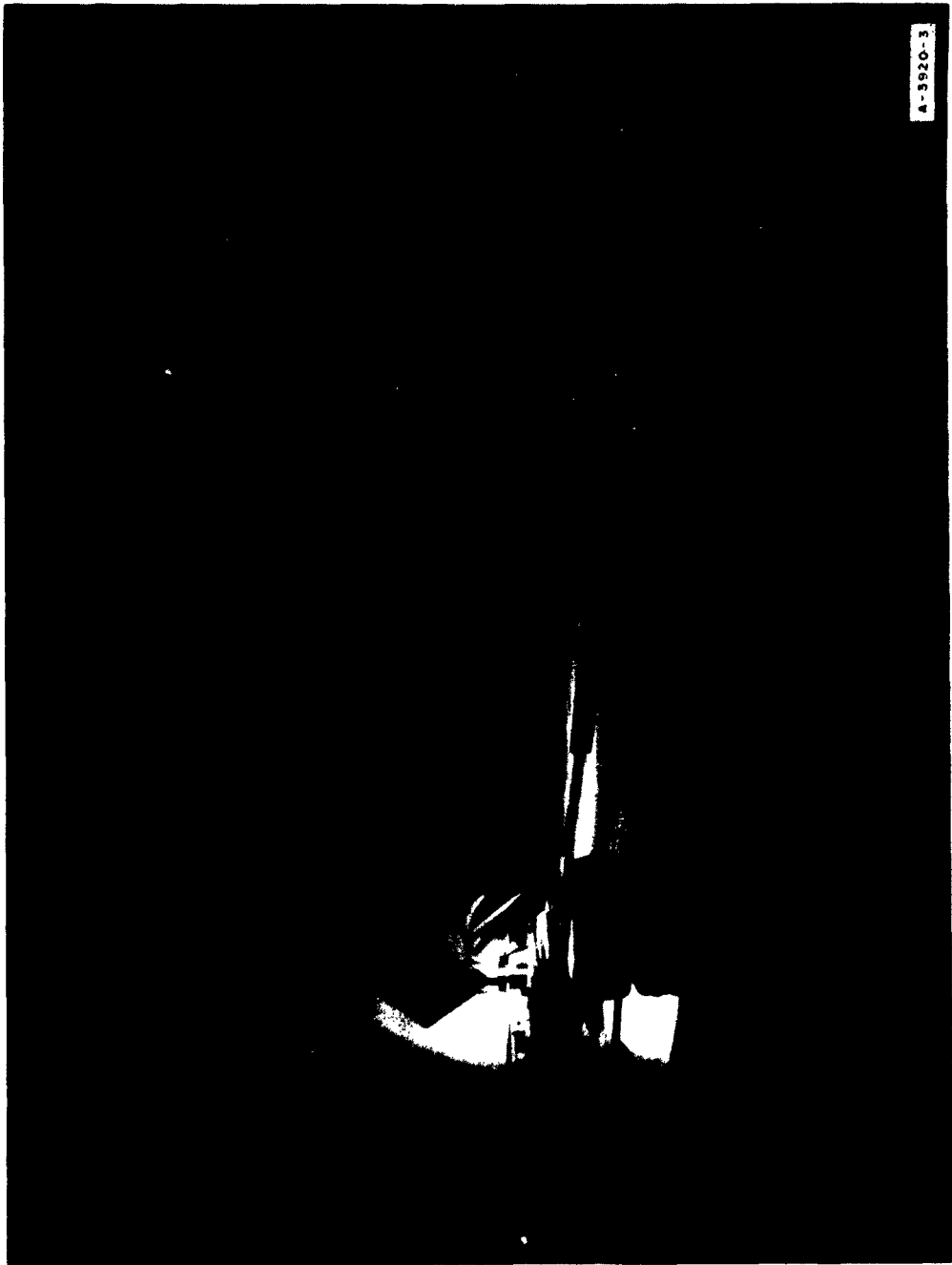


Figure 2



Schematic diagram of arc image furnace

Figure 3

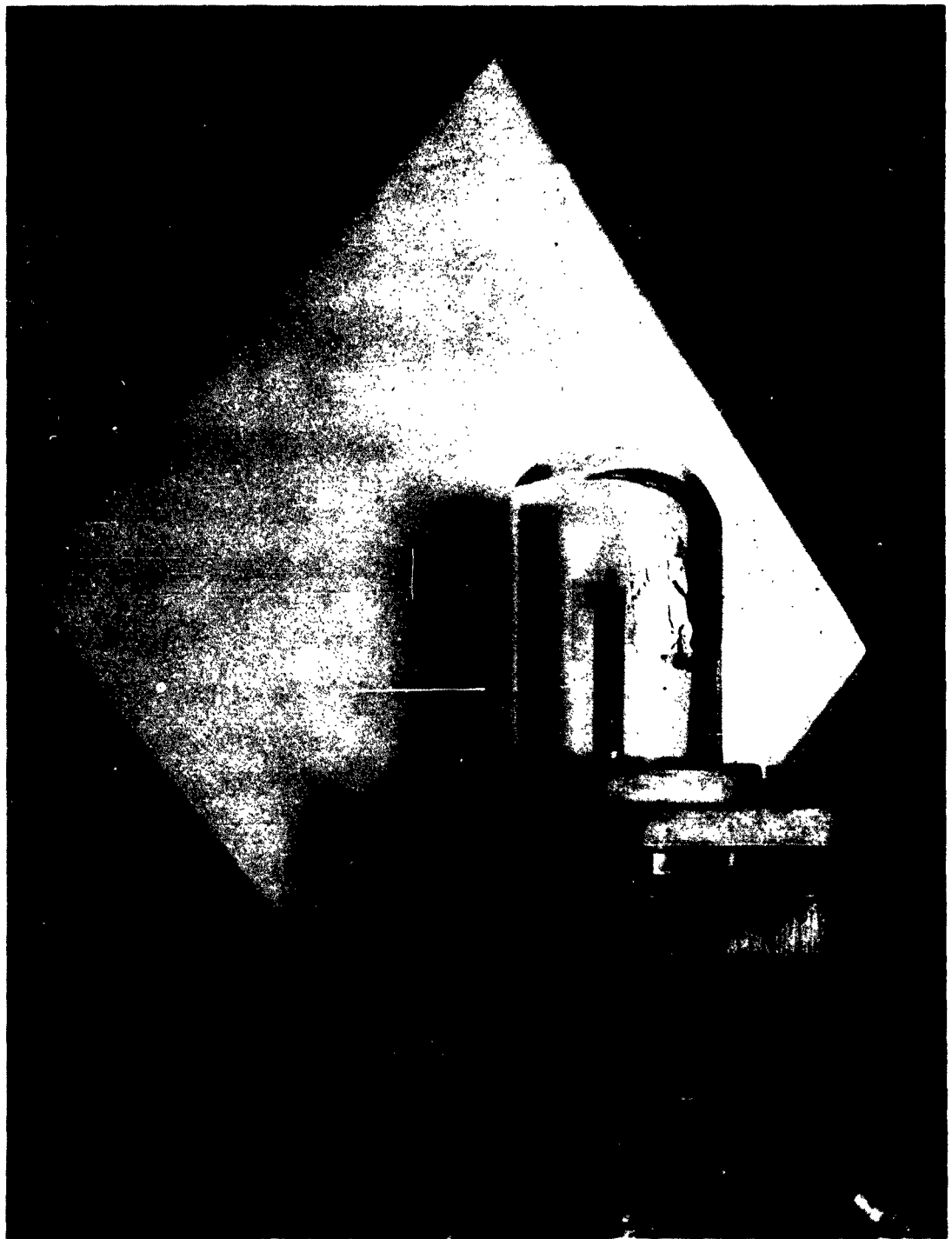


Arc image furnace and auxiliary equipment
Figure 4



Adjustable diaphragm

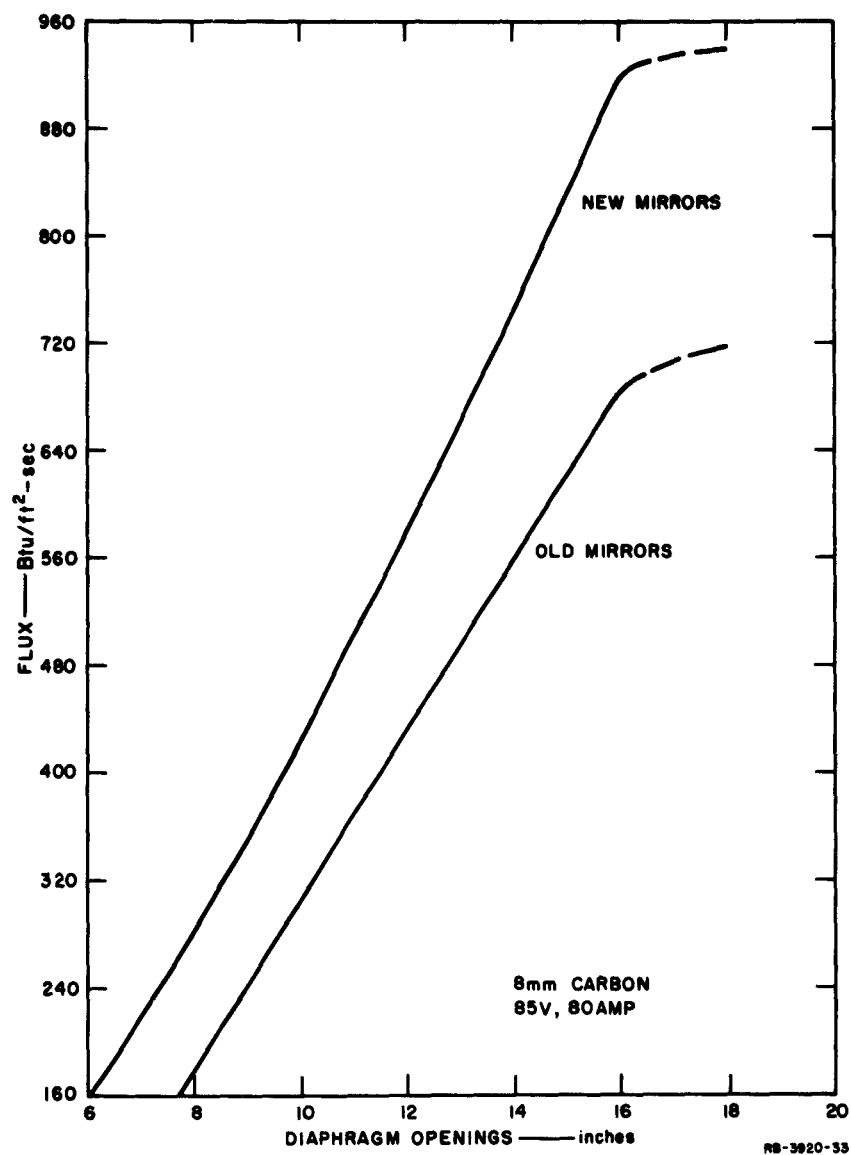
Figure 5



High pressure container
Figure 6



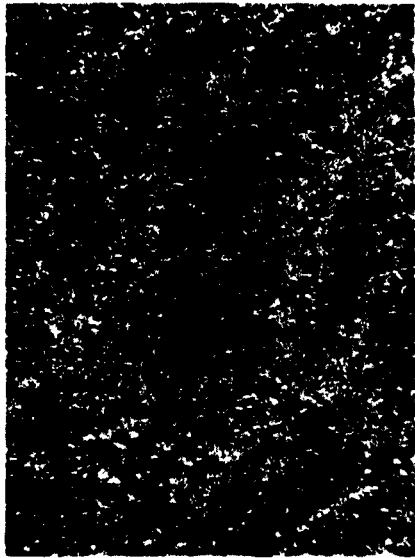
Typical sample
Figure 7



Calibration curve for arc image furnace
Figure 8



100μ



25μ

MATERIAL: ALLOY (90% Zr - 10% U) BEFORE HEATING

P-3920-20

Zirconium -- 10% uranium alloy

Figure 9



100 μ



25 μ

MATERIAL: HYDRIDED Zr-U ALLOY BEFORE HEATING

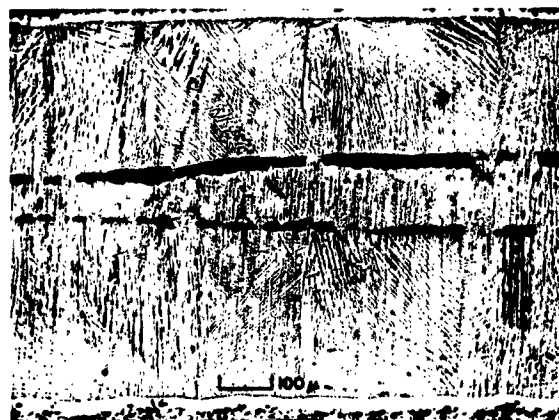
Hydried zirconium -- uranium alloy

Figure 10

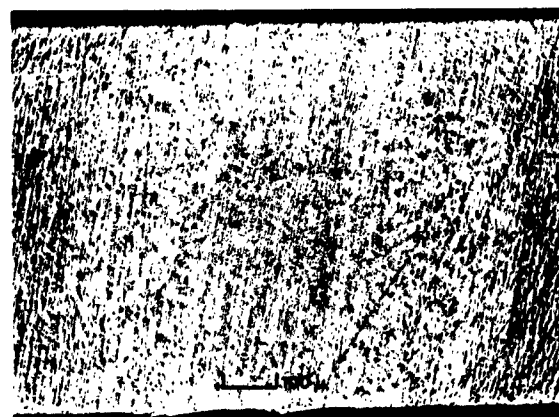
P-3920-21



(a)

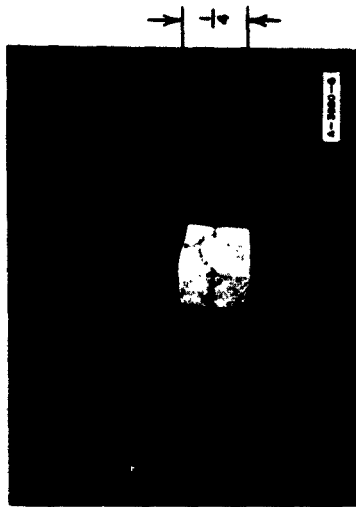


(b)



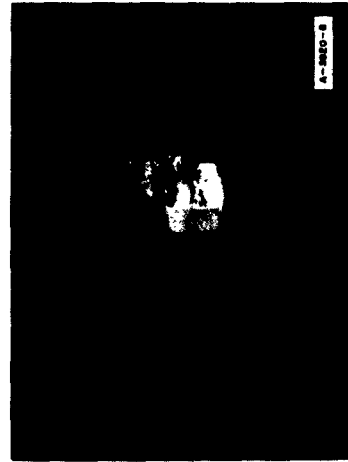
(c)

Photomicrographs of heated and oxidized zirconium
Figure 11



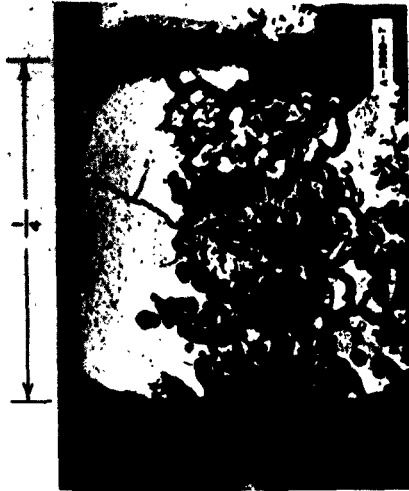
ZIRCONIUM-URANIUM ALLOY
AFTER HEATING

Figure 12a



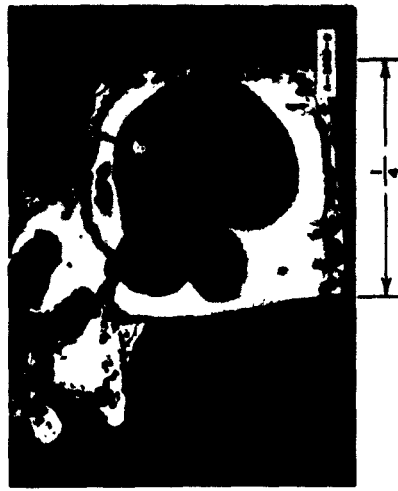
ZIRCONIUM-URANIUM HYDRIDE
AFTER HEATING

Figure 13a



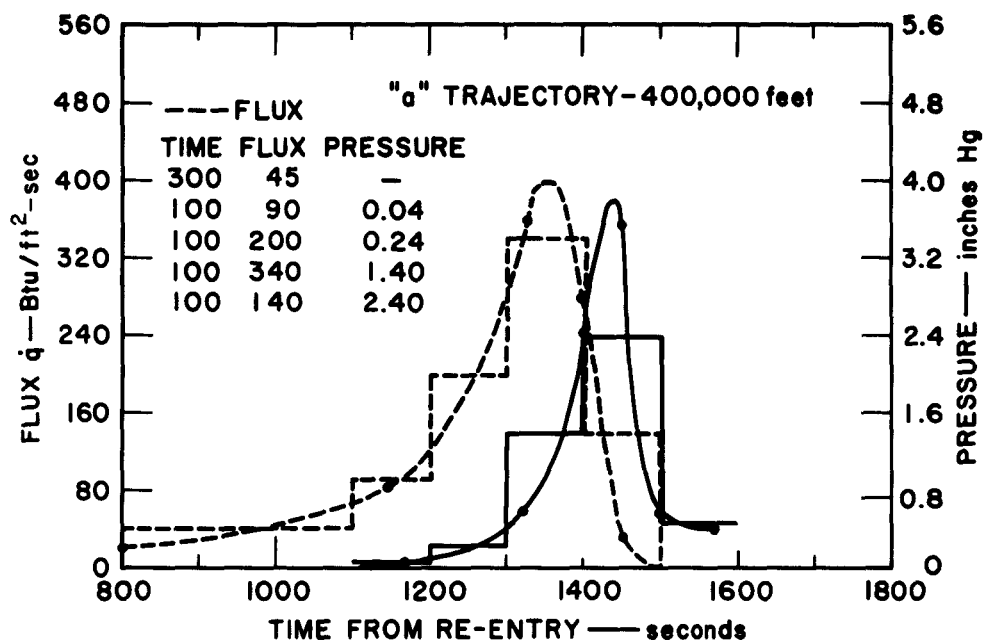
ZIRCONIUM-URANIUM ALLOY
AFTER HEATING (Section)

Figure 12b



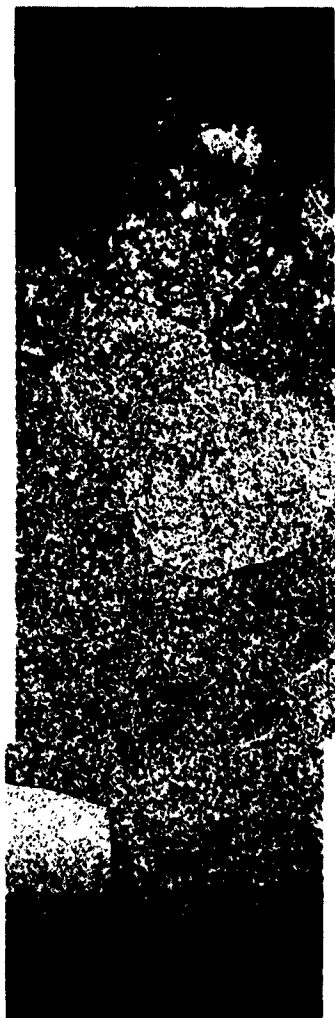
ZIRCONIUM-URANIUM HYDRIDE
AFTER HEATING (Section)

Figure 13b



B - 3920 - 12

Figure 14



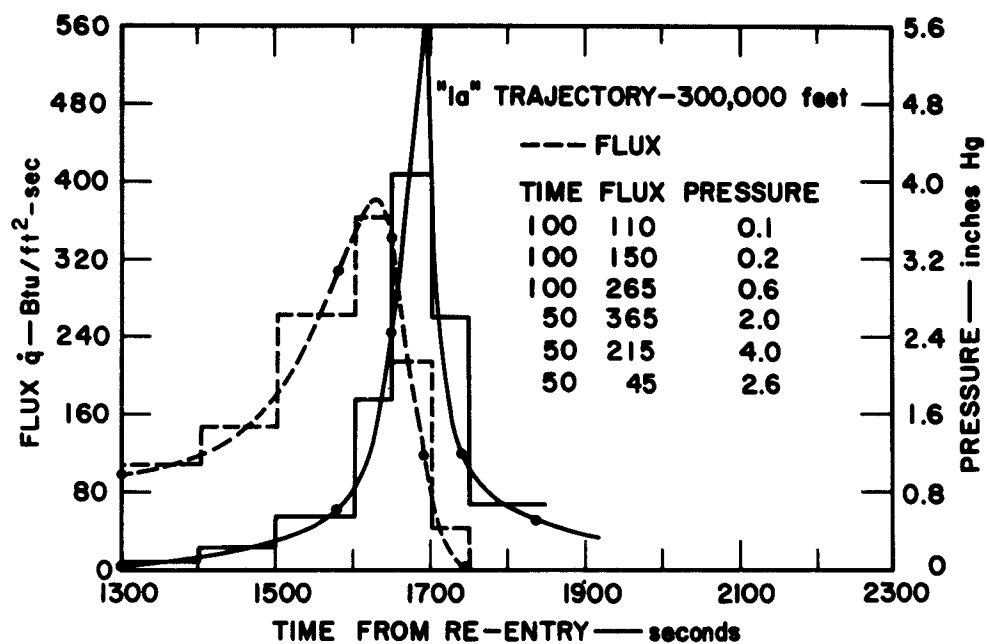
TRAJECTORY: a MATERIAL: ALLOY RUN No.: a-7 135μ



TRAJECTORY: a MATERIAL: HYDRIDE RUN No.: a-9 135μ

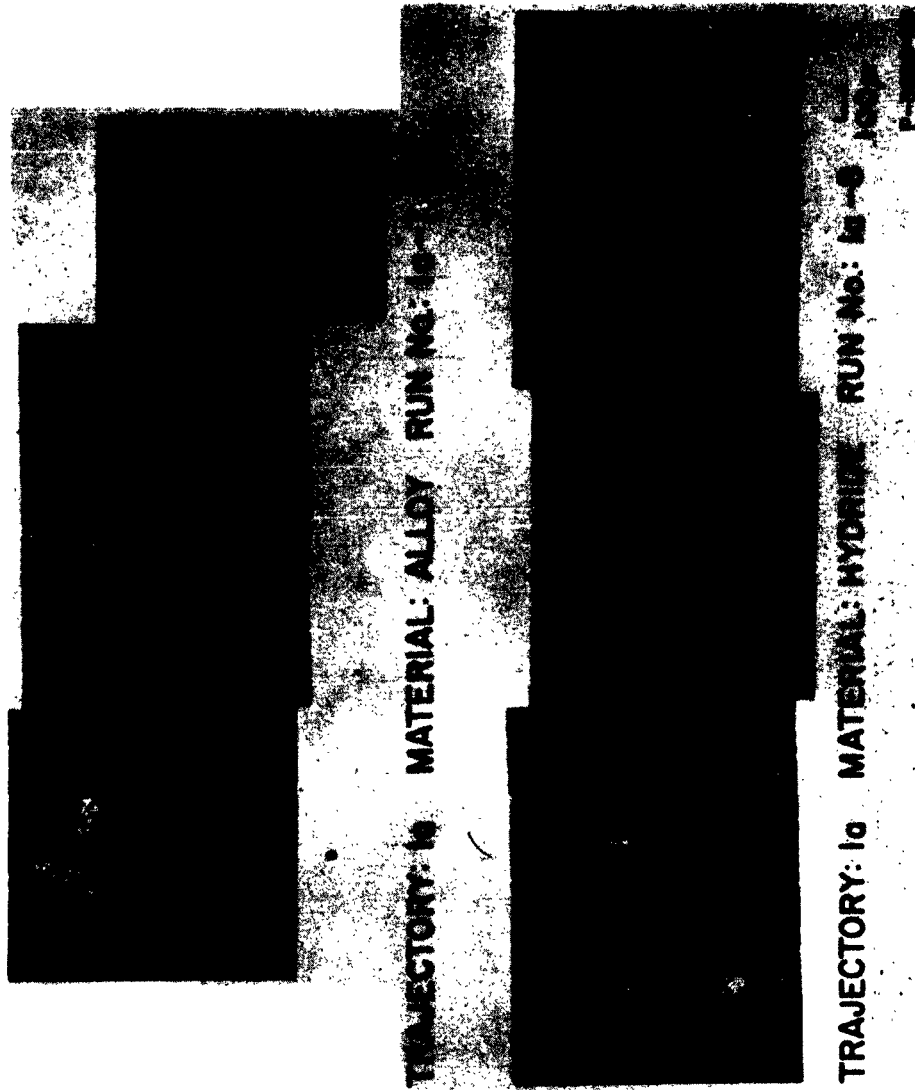
P-3920-16

Samples of material from "a" trajectory
Figure 15

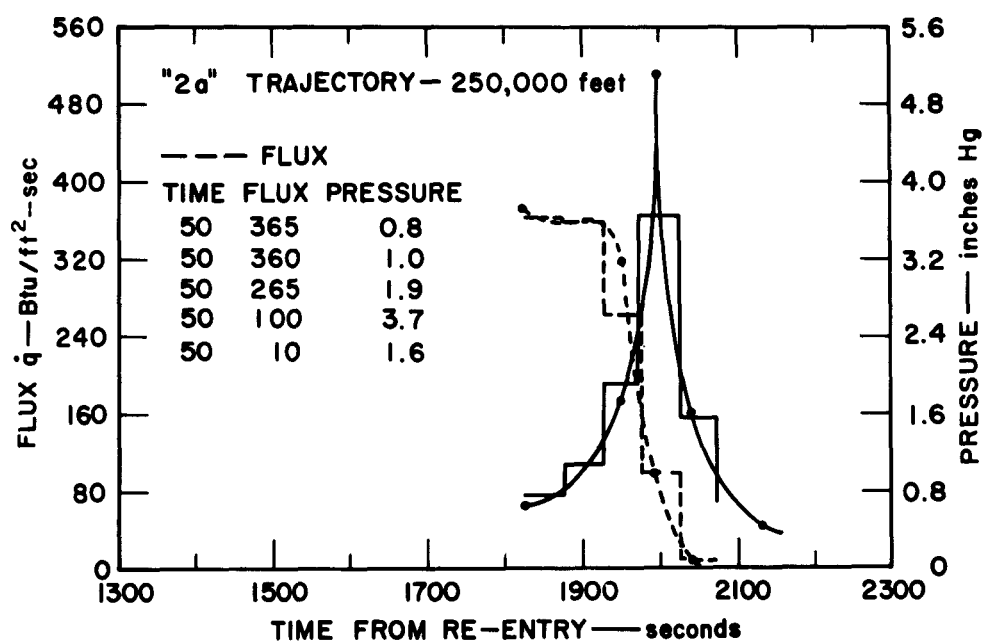


8-3920-13

Figure 16



Samples of material from "la" trajectory
Figure 17



8-3920-14

Figure 18



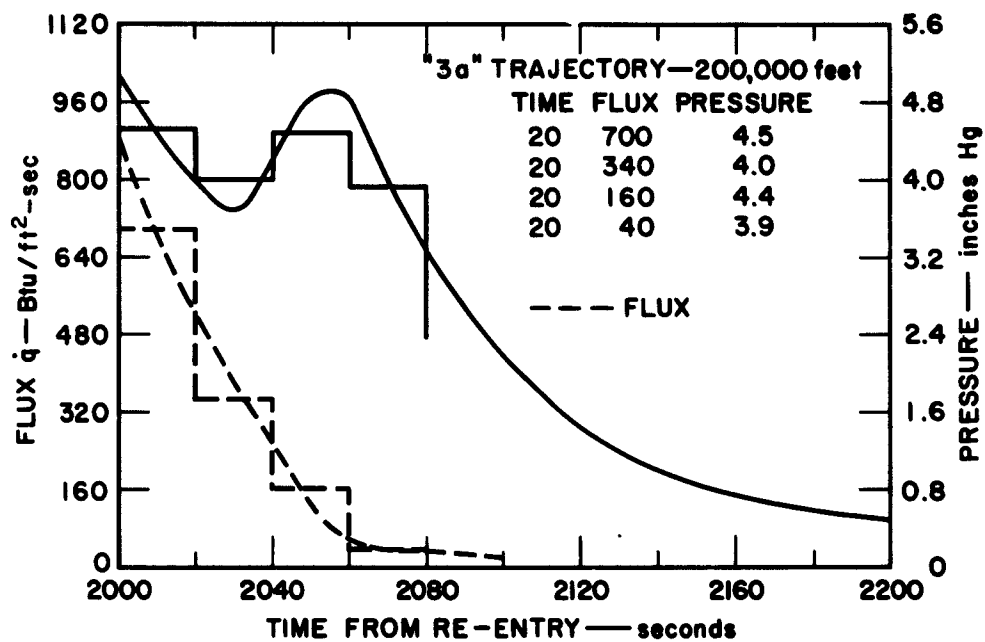
TRAJECTORY: 2a MATERIAL: ALLOY RUN No.: 2a-7 135μ



TRAJECTORY: 2a MATERIAL: HYDRIDE RUN No.: 2a-8 135μ

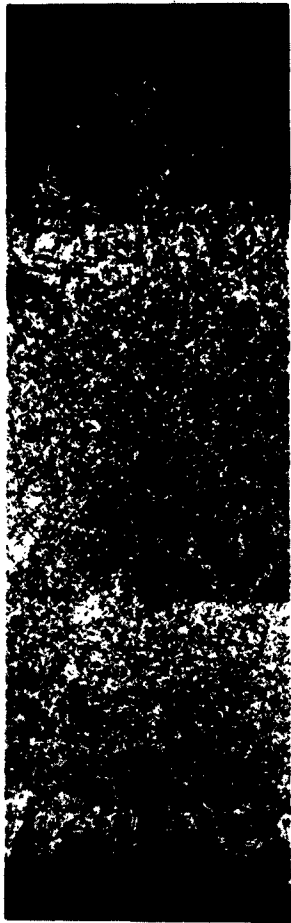
P-3920-17

Samples of material from "2a" trajectory
Figure 19



B-3920-16

Figure 2.0



TRAJECTORY: 3a . MATERIAL: ALLOY 3a-2 135μ



TRAJECTORY: 3a MATERIAL: HYDRIDE 3a-3 135μ

P-3920-22

Sample of material from "3a" trajectory at average stagnation flux
Figure 21



135μ

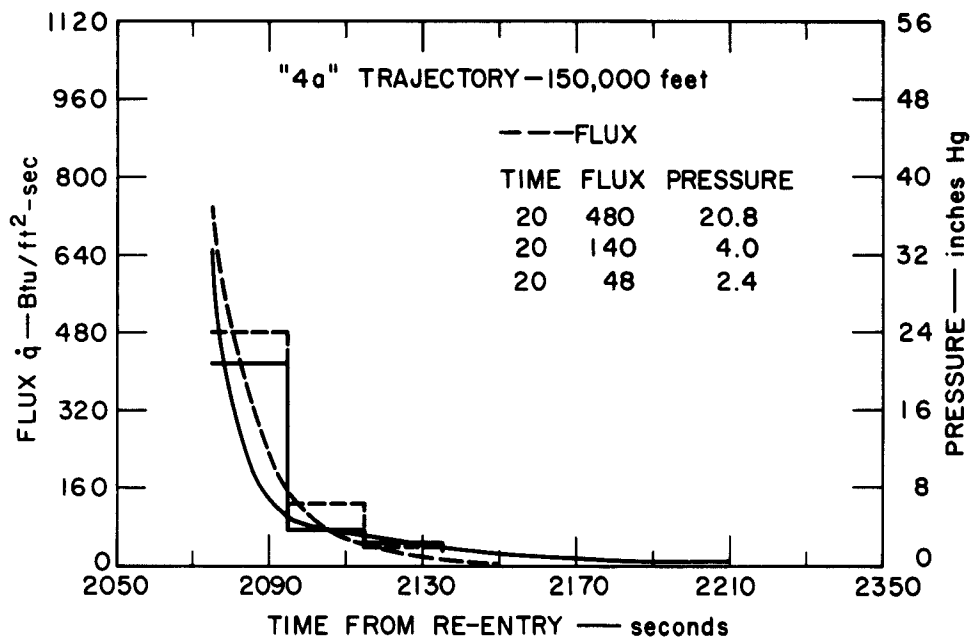
TRAJECTORY: 3a MATERIAL: ALLOY SAMPLE NO: 6



135μ

TRAJECTORY: 3a MATERIAL: HYDRIDE SAMPLE NO: 8

Samples of material from "3a" trajectory at increased flux
Figure 22



RB-3920-15

Figure 23



135μ

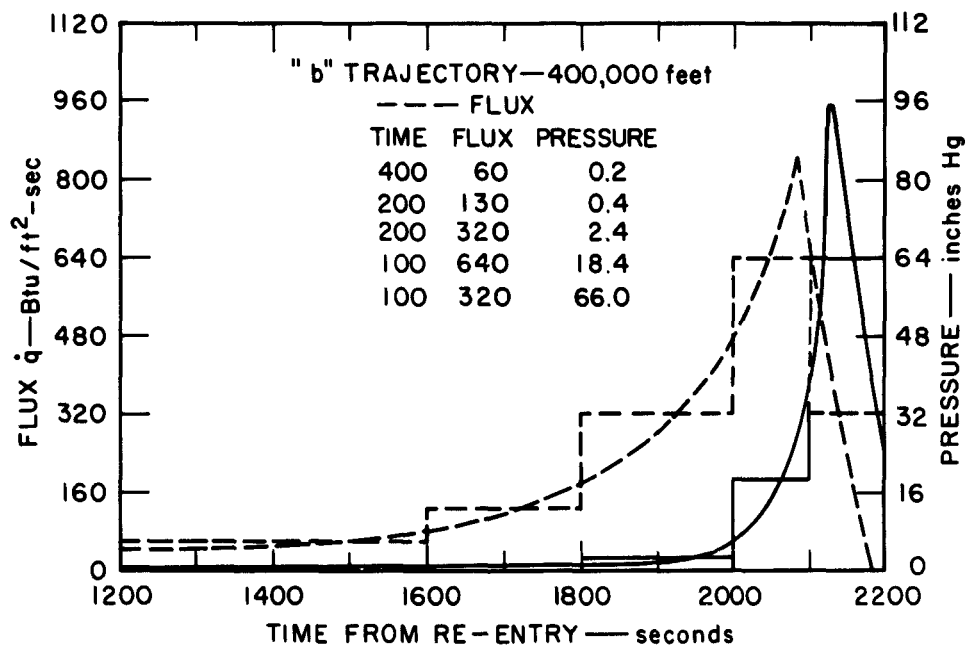
TRAJECTORY: 4a MATERIAL: ALLOY SAMPLE NO.: 5



135μ

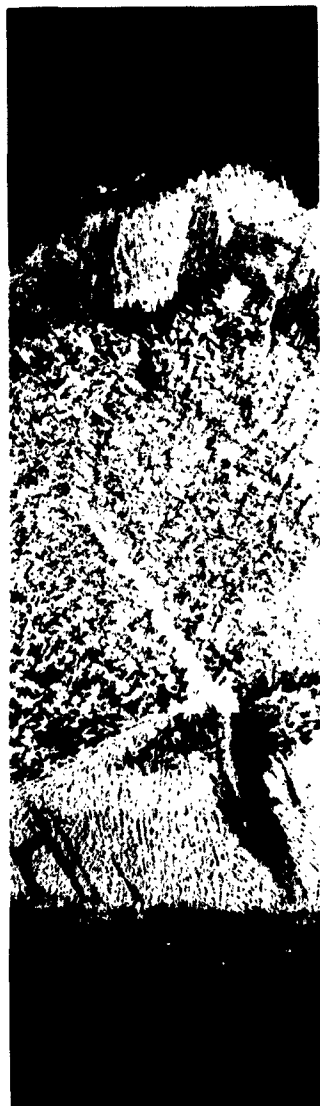
TRAJECTORY: 4a MATERIAL: HYDRIDE SAMPLE NO.: 8

Samples of material from "4a" trajectory
Figure 24



RB-3920-27

Figure 25



TRAJECTORY: b MATERIAL: ALLOY SAMPLE NO.: 6

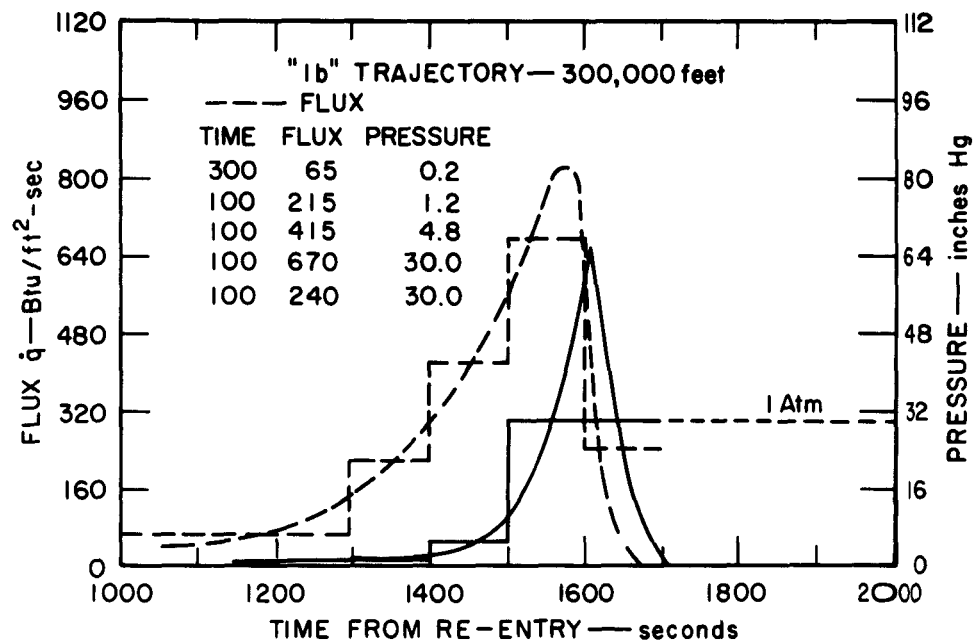
135 μ



TRAJECTORY: b MATERIAL: HYDRIDE SAMPLE NO.: 8

135 μ

Samples of material from "b" trajectory
Figure 26



RB-3920-26

Figure 27



TRAJECTORY : 1b MATERIAL : ALLOY SAMPLE No. : 5 135μ



TRAJECTORY : 1b MATERIAL : HYDRIDE SAMPLE No. : 7 135μ

P-3920-32

Samples of material from "1b" trajectory
Figure 28

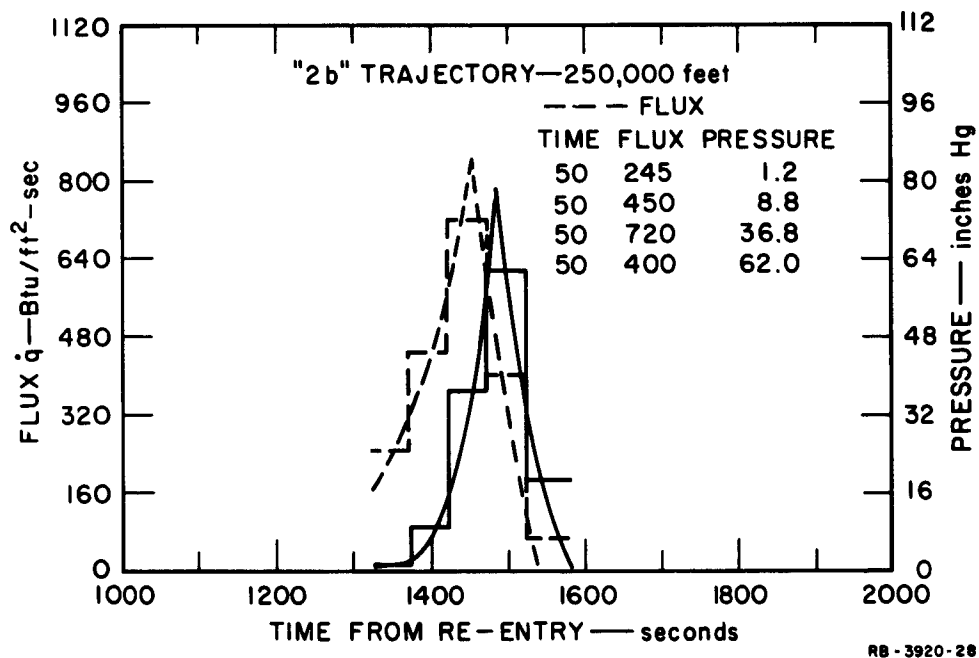


Figure 29

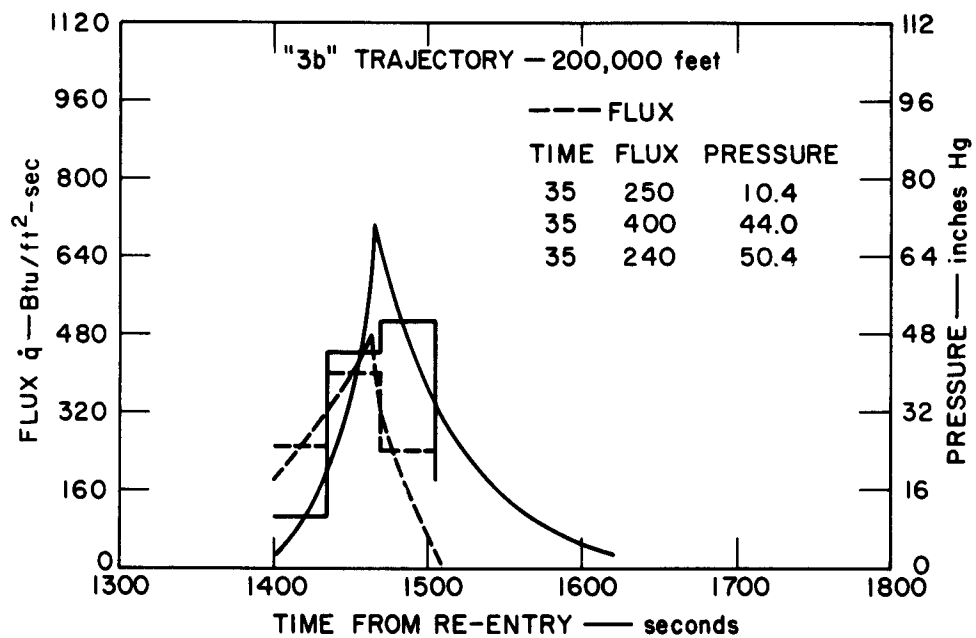


TRAJECTORY : 2b MATERIAL : ALLOY SAMPLE No. : 2 \square 135 μ



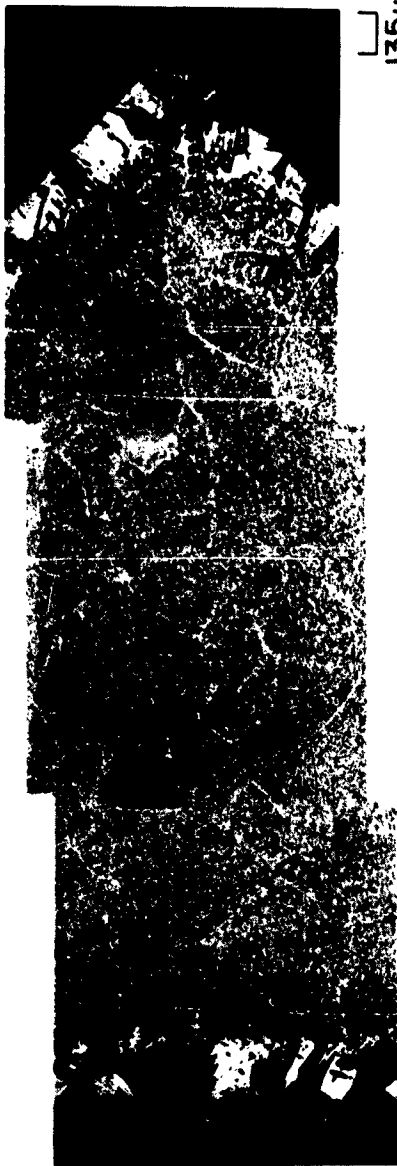
TRAJECTORY : 2b MATERIAL : HYDRIDE SAMPLE No. : 4 \square 135 μ
P-3920-30

Samples of material from "2b" trajectory
Figure 30



RB-3920-24

Figure 31



135 μ

TRAJECTORY : 3b MATERIAL : ALLOY SAMPLE No. : 2

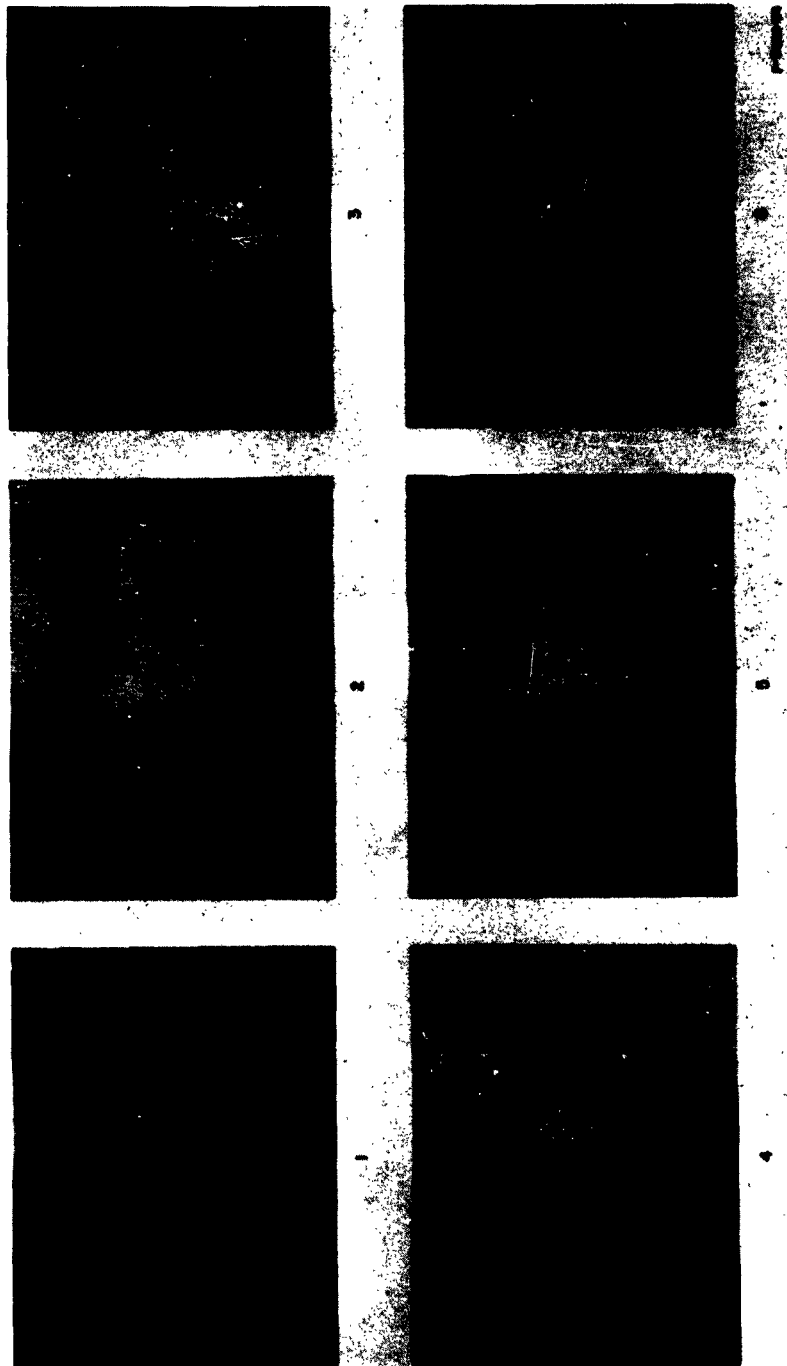


135 μ

TRAJECTORY : 3b MATERIAL : HYDRIDE SAMPLE No. : 4
P-3920-3I

Samples of material from "3b" trajectory

Figure 32



Formation of water
Figure 33

DISTRIBUTION

No. cys

HEADQUARTERS USAF

1	Hq USAF (AFRST), Wash 25, DC
1	USAF Dep, The Inspector General (AFIDI), Norton AFB, Calif
1	USAF Directorate of Nuclear Safety (AFINS), Kirtland AFB, NM

MAJOR AIR COMMANDS

1	AFSC (SCCP), Andrews AFB, Wash 25, DC
1	AUL, Maxwell AFB, Ala

AFSC ORGANIZATIONS

1	ASD (ASRMFP), Wright-Patterson AFB, Ohio
1	RTD (RTO), Bolling AFB, Wash 25, DC
	SSD, AF Unit Post Office, Los Angeles 45, Calif
1	(SSTRE)
1	(SSZMS)

KIRTLAND AFB ORGANIZATIONS

	AFSWC, Kirtland AFB, NM
1	(SWEH)
83	(SWOI)
1	(SWRP)
2	(SWVPS)
2	(SWVPF)
1	US Naval Weapons Evaluation Facility (NWEF) (Code 404) Kirtland AFB, NM

OTHER AIR FORCE AGENCIES

1	Director, USAF Project RAND, via: Air Force Liaison Office, The RAND Corporation (Miss Mary Romig), 1700 Main Street, Santa Monica, Calif
---	---

DISTRIBUTION (cont'd)

No. cys

OTHER DOD ACTIVITIES

Director, Advanced Research Projects Agency, Department of
Defense, The Pentagon, Wash 25, DC

2 (Lt Col Roy Weidler)

2 (James E. Blower)

10 ASTIA (TIPDR), Arlington Hall Sta, Arlington 12, Va

AEC ACTIVITIES

US Atomic Energy Commission, Wash 25, DC

4 (DRD/Assistant Director for Compact Reactor Systems)

4 (DRD/Assistant Director for Nuclear Safety)

6 Sandia Corporation, ATTN: Mr. V. E. Blake, Dept 7110,
Sandia Base, NM

1 US Atomic Energy Commission, ATTN: Mr. J. Levy, Canoga
Park Area, Canoga Park, Calif

1 University of California Lawrence Radiation Laboratory
(Technical Information Division), P.O. Box 808, Livermore,
Calif

OTHER

1 OTS, Department of Commerce, Wash 25, DC

3 Battelle Memorial Institute, ATTN: E. L. Foster, 505 King
Avenue, Columbus, Ohio

1 Institute of the Aerospace Sciences, Inc., 2 East 64th Street,
New York 21, NY

6 Aerospace Corporation, Library Technical Documents Group,
ATD61-5729, Tech Info Ctr, P. O. Box 95085, Los Angeles 45,
Calif

10 General Dynamics/Astronautics, ATTN: Mr. E. J. Philbin,
P.O. Box 1128, Mail Zone 596-2, San Diego 12, Calif





6 Stanford Research Institute, Menlo Park, Calif

DISTRIBUTION (cont'd)

No. cys

3	Vidya Research and Development, ATTN: Mr. W. J. Fleming, 2626 Hanover Street, Palo Alto, Calif
3	Astropower, ATTN: Dr. A. E. Levy-Pascal, 2968 Randolph Avenue, Costa Mesa, Calif
3	Armour Research Foundation, ATTN: Mr. Jack Hedge, 10 West 35th Street, Chicago 16, Ill
10	Space Information Systems Division, North American Aviation, Inc., ATTN: Mr. Mark Morris, Department 468, 12214 Lakewood Blvd., Downey, Calif
3	General Technology Corporation, ATTN: Mr. J. D. Graves, 2302 Willowood Lane, Alexandria, Va
3	AVCO Corporation, ATTN: Dr. J. G. Lundholm, 201 Lowell Street, Wilmington, Mass
3	Westinghouse Electric Corp., Astronuclear Laboratory, ATTN: Mr. Alexander L. Feild, Jr., 250 Mt Lebanon Blvd., Pittsburgh, Pa
1	Official Record Copy (SWVPF, Mr. J. J. Ungvarsky)

<p>Air Force Special Weapons Center, Kirtland AF Base, New Mexico</p> <p>Rpt. No. AFSC-TDR-63-15. ZIRCONIUM -- URANIUM COMBUSTION STUDY. Final Report, April 1963. 62 p. incl illus, tables. Unclassified Report</p> <p>This investigation was designed to provide an experimental verification of the melting and oxidation behavior of fuel rod material of the type used in SNAP-2 and SNAP-10A auxiliary power reactors. Samples of zirconium-uranium alloy, both hydrided and unhydrided, were subjected to static conditions approximating reentry trajectories. Heat flux and pressure conditions encountered during reentry were selected to bracket ballistic parameter ranges of $W/C_p A = 20$ to $W/C_p A = 300$ and altitude ranges of 400,000 to 150,000 feet. An arc image furnace capable of delivering up to</p>	<p>Heat transfer</p> <p>Pressure</p> <p>Radiation hazards</p> <p>Reactor fuels -- oxidation and reduction</p> <p>Reentry</p> <p>SNAP</p> <p>Structural elements</p> <p>Trajectories -- simulation</p> <p>Uranium alloys -- oxidation and reduction</p> <p>Zirconium alloys -- oxidation and reduction</p> <p>AFSC Project 1831, Task 183101</p> <p>Contract AF 29(601)-4954</p> <p>Stanford Research Inst. Menlo Park, Calif</p> <p>Fred E. Littman</p>	<p>1. Heat transfer</p> <p>2. Pressure</p> <p>3. Radiation hazards</p> <p>4. Reactor fuels -- oxidation and reduction</p> <p>5. Reentry</p> <p>6. SNAP</p> <p>7. Structural elements</p> <p>8. Trajectories -- simulation</p> <p>9. Uranium alloys -- oxidation and reduction</p> <p>10. Zirconium alloys -- oxidation and reduction</p> <p>I. AFSC Project 1831, Task 183101</p> <p>II. Contract AF 29(601)-4954</p> <p>III. Stanford Research Inst. Menlo Park, Calif</p> <p>IV. Fred E. Littman</p>
<p>Air Force Special Weapons Center, Kirtland AF Base, New Mexico</p> <p>Rpt. No. AFSC-TDR-63-15. ZIRCONIUM -- URANIUM COMBUSTION STUDY. Final Report, April 1963. 62 p. incl illus, tables. Unclassified Report</p> <p>This investigation was designed to provide an experimental verification of the melting and oxidation behavior of fuel rod material of the type used in SNAP-2 and SNAP-10A auxiliary power reactors. Samples of zirconium-uranium alloy, both hydrided and unhydrided, were subjected to static conditions approximating reentry trajectories. Heat flux and pressure conditions encountered during reentry were selected to bracket ballistic parameter ranges of $W/C_p A = 20$ to $W/C_p A = 300$ and altitude ranges of 400,000 to 150,000 feet. An arc image furnace capable of delivering up to</p>	<p>Heat transfer</p> <p>Pressure</p> <p>Radiation hazards</p> <p>Reactor fuels -- oxidation and reduction</p> <p>Reentry</p> <p>SNAP</p> <p>Structural elements</p> <p>Trajectories -- simulation</p> <p>Uranium alloys -- oxidation and reduction</p> <p>Zirconium alloys -- oxidation and reduction</p> <p>AFSC Project 1831, Task 183101</p> <p>Contract AF 29(601)-4954</p> <p>Stanford Research Inst. Menlo Park, Calif</p> <p>Fred E. Littman</p>	<p>1. Heat transfer</p> <p>2. Pressure</p> <p>3. Radiation hazards</p> <p>4. Reactor fuels -- oxidation and reduction</p> <p>5. Reentry</p> <p>6. SNAP</p> <p>7. Structural elements</p> <p>8. Trajectories -- simulation</p> <p>9. Uranium alloys -- oxidation and reduction</p> <p>10. Zirconium alloys -- oxidation and reduction</p> <p>I. AFSC Project 1831, Task 183101</p> <p>II. Contract AF 29(601)-4954</p> <p>III. Stanford Research Inst. Menlo Park, Calif</p> <p>IV. Fred E. Littman</p>
<p>Air Force Special Weapons Center, Kirtland AF Base, New Mexico</p> <p>Rpt. No. AFSC-TDR-63-15. ZIRCONIUM -- URANIUM COMBUSTION STUDY. Final Report, April 1963. 62 p. incl illus, tables. Unclassified Report</p> <p>This investigation was designed to provide an experimental verification of the melting and oxidation behavior of fuel rod material of the type used in SNAP-2 and SNAP-10A auxiliary power reactors. Samples of zirconium-uranium alloy, both hydrided and unhydrided, were subjected to static conditions approximating reentry trajectories. Heat flux and pressure conditions encountered during reentry were selected to bracket ballistic parameter ranges of $W/C_p A = 20$ to $W/C_p A = 300$ and altitude ranges of 400,000 to 150,000 feet. An arc image furnace capable of delivering up to</p>	<p>Heat transfer</p> <p>Pressure</p> <p>Radiation hazards</p> <p>Reactor fuels -- oxidation and reduction</p> <p>Reentry</p> <p>SNAP</p> <p>Structural elements</p> <p>Trajectories -- simulation</p> <p>Uranium alloys -- oxidation and reduction</p> <p>Zirconium alloys -- oxidation and reduction</p> <p>AFSC Project 1831, Task 183101</p> <p>Contract AF 29(601)-4954</p> <p>Stanford Research Inst. Menlo Park, Calif</p> <p>Fred E. Littman</p>	<p>1. Heat transfer</p> <p>2. Pressure</p> <p>3. Radiation hazards</p> <p>4. Reactor fuels -- oxidation and reduction</p> <p>5. Reentry</p> <p>6. SNAP</p> <p>7. Structural elements</p> <p>8. Trajectories -- simulation</p> <p>9. Uranium alloys -- oxidation and reduction</p> <p>10. Zirconium alloys -- oxidation and reduction</p> <p>I. AFSC Project 1831, Task 183101</p> <p>II. Contract AF 29(601)-4954</p> <p>III. Stanford Research Inst. Menlo Park, Calif</p> <p>IV. Fred E. Littman</p>

<p>900 BTU/ft²-sec was used as a source of radiant flux.</p> <p>The results suggest that under these conditions no melting of the fuel rods is likely to occur. The material lost hydrogen and became almost completely oxidized. The resulting material, though mechanically weaker and more brittle than the starting material, was also extremely refractory owing to the high melting point of the zirconium oxide.</p> 	<p>V. SRI Project PMU-3920 VI. In ASTIA collection</p>	<p>900 BTU/ft²-sec was used as a source of radiant flux.</p> <p>The results suggest that under these conditions no melting of the fuel rods is likely to occur. The material lost hydrogen and became almost completely oxidized. The resulting material, though mechanically weaker and more brittle than the starting material, was also extremely refractory owing to the high melting point of the zirconium oxide.</p> 	<p>V. SRI Project PMU-3920 VI. In ASTIA collection</p>
<p>900 BTU/ft²-sec was used as a source of radiant flux.</p> <p>The results suggest that under these conditions no melting of the fuel rods is likely to occur. The material lost hydrogen and became almost completely oxidized. The resulting material, though mechanically weaker and more brittle than the starting material, was also extremely refractory owing to the high melting point of the zirconium oxide.</p> 	<p>V. SRI Project PMU-3920 VI. In ASTIA collection</p>	<p>900 BTU/ft²-sec was used as a source of radiant flux.</p> <p>The results suggest that under these conditions no melting of the fuel rods is likely to occur. The material lost hydrogen and became almost completely oxidized. The resulting material, though mechanically weaker and more brittle than the starting material, was also extremely refractory owing to the high melting point of the zirconium oxide.</p> 	<p>V. SRI Project PMU-3920 VI. In ASTIA collection</p>